

# 1 **Technical Note: Lessons from and best practices for the** 2 **deployment of the Soil Water Isotope Storage System**

3 Rachel E. Havranek<sup>1</sup>, Kathryn Snell<sup>1</sup>, Sebastian Kopf<sup>1</sup>, Brett Davidheiser-Kroll<sup>2</sup>, Valerie Morris<sup>3</sup>, Bruce  
4 Vaughn<sup>3</sup>

5 Rachel Havranek, Kathryn Snell, Sebastian Kopf, Brett Davidheiser-Kroll, Valerie Morris, Bruce Vaughn

6 <sup>1</sup>Geological Sciences, University of Colorado Boulder, Boulder, 80303, USA

7 <sup>2</sup>Thermo Fisher Scientific (Bremen) GmbH, Bremen, Germany

8 <sup>3</sup>Institute of Arctic and Alpine Research, University of Colorado Boulder, Boulder, 80303, USA

9 *Correspondence to:* Rachel Havranek (rachel.havranek@colorado.edu)

10 **Abstract.** Soil water isotope datasets are useful for understanding connections between the  
11 hydrosphere, atmosphere, biosphere, and geosphere. However, they have been underproduced  
12 because of technical challenges associated with collecting those datasets. Here, we present the  
13 results of testing and automation of the Soil Water Isotope Storage System (SWISS). The unique  
14 innovation of the SWISS is that we are able to automatically collect water vapor from the critical  
15 zone at a regular time interval and then store that water vapor until it can be measured back in a  
16 laboratory setting. Through a series of quality assurance and quality control tests, we tested that  
17 the SWISS is resistant to both atmospheric intrusion and leaking in both laboratory and field  
18 settings. We assessed the accuracy and precision of the SWISS through a series of experiments  
19 where water vapor of known composition was introduced into the flasks, stored for 14 days, and  
20 then measured. From these experiments, after applying an offset correction to report our values  
21 relative to VSMOW/SLAP, we assess the precision of the SWISS at  $\pm 0.9\text{‰}$  and  $\pm 3.7\text{‰}$  for  $\delta^{18}\text{O}$   
22 and  $\delta^2\text{H}$ , respectively. We deployed three SWISS units to three different field sites to  
23 demonstrate that the SWISS stores water vapor reliably enough that we are able to differentiate  
24 dynamics both between the sites as well within a single soil column. Overall, we demonstrate  
25 that the SWISS retains the stable isotope composition of soil water vapor for long enough to  
26 allow researchers to address a wide range of ecohydrologic questions.

## 27 **1 Introduction**

28 Understanding soil water dynamics across a range of environments and soil properties is  
29 critical to food and water security (e.g. Mahindawansa et al., 2018; Quade et al., 2019; Rothfuss  
30 et al., 2021); understanding biogeochemical cycles, such as the nitrogen and phosphorus cycles  
31 (e.g. Hinckley et al., 2014; Harms and Ludwig, 2016); and understanding connections between  
32 the hydrosphere, biosphere, geosphere and atmosphere (e.g. Vereeken et al., 2022). One  
33 approach that can be used to understand water use and movement in the critical zone is the stable  
34 isotope geochemistry of soil water (e.g. Sprenger et al., 2016; Bowen et al., 2019). Variations in  
35 the stable isotope ratios of oxygen and hydrogen of soil water ( $\delta^{18}\text{O}$ ,  $\delta^2\text{H}$ ) track physical  
36 processes like infiltration, root water uptake and evaporation. In particular, stable water isotopes  
37 are useful for disentangling complex mixtures of water from multiple sources (e.g. Dawson and  
38 Ehleringer, 1991; Brooks et al., 2010; Soderberg et al., 2012; Good et al., 2015; Bowen et al.,  
39 2018; Gomez-Navarro et al., 2019; Sprenger and Allen 2020). Despite the long-recognized  
40 utility of measuring soil water isotopes for understanding a range of processes (e.g. Zimmerman

41 et al., 1966; Peterson & Fry., 1987), soil water isotope datasets have been under-produced as  
42 compared to groundwater and meteoric water isotope datasets (Bowen et al., 2019).

43 The primary barrier to producing soil water isotope datasets has been the arduous nature  
44 of collecting samples. Historically, there are two primary methods for collecting soil water  
45 samples: either digging a pit and collecting a mass of soil to bring back to the lab for subsequent  
46 water extraction or via lysimeter. The former method disrupts the soil profile each time a sample  
47 is collected, inhibiting the creation of long-term records of soil water isotopes. Lysimeters on the  
48 other hand provide the means to collect multi-year soil water isotope datasets (e.g. Stumpp et al.,  
49 2012, Zhao et al., 2013; Hinkley et al., 2014; Green et al., 2015; Groh et al., 2018 ), but the  
50 choice of lysimeter can affect the portion of soil water (i.e. mobile vs. bound) that is sampled  
51 (Hinkley et al., 2014; Sprenger et al., 2015) and the soil conditions that are sampleable (i.e.  
52 saturation state). Soil water samples collected from both bulk soil samples and lysimeters often  
53 require manual intervention at the time of sampling.

54 Building off of innovations in laser-based spectroscopy for stable isotope geochemistry,  
55 the ecohydrology community developed a variety of in situ soil water sampling methods over the  
56 last 15 years that enable the creation of high throughput, high precision analyses of soil water  
57 isotopes (e.g. Wassenaar et al., 2008; Gupta et al. 2009; Rothfuss et al., 2013; Volkmann and  
58 Weiler, 2014; Gaj et al., 2015; Oerter et al., 2016; Beyer et al., 2020; Kübert et al., 2020). These  
59 methods have provided insights into a range of ecohydrologic questions from evaporation and  
60 water use dynamics in managed soils (e.g. Oerter et al., 2017; Quade et al., 2018) to better  
61 understanding where plants and trees source their water (e.g. Beyer et al., 2020). These  
62 innovations have allowed researchers to ask new questions about ecohydrologic dynamics, but  
63 current methods require field deployments of laser-based instruments. Field deployments are  
64 technically possible and have been conducted successfully (e.g. Gaj et al., 2016; Volkmann et al.,  
65 2016; Oerter et al., 2017; Quade et al., 2019; Künhammer et al., 2021; Seeger and Weiler., 2021;  
66 Gessler et al., 2022), but require uninterrupted AC power, adequate shelter, as well as safe and  
67 stable operating environments for best results. These prerequisites are often unavailable at many  
68 field sites, especially in more remote locations and for longer sampling time frames. Given these  
69 logistical constraints, these studies have mostly been done near the institutions performing those  
70 studies. Spatial constraints limit the questions that researchers can ask about soil hydrology in  
71 remote and traditionally understudied landscapes. For example, in the geoscience community  
72 there is significant interest in improving the research community's understanding of how and  
73 when paleoclimate proxies (e.g. stable isotope records from pedogenic carbonate, branched  
74 glycerol dialkyl glycerol tetraethers, etc.) form in soils, because that informs our ability to  
75 accurately interpret records from the geologic past. However, those projects commonly have  
76 environmental constraints like soil type or local climate characteristics that may not be located  
77 near institutions performing those studies. To be able to study a broader range of questions about  
78 ecohydrology, there is a need for a system that is capable of autonomously collecting soil water  
79 vapor for isotopic analysis in remote settings.

80 In this contribution, we report on the further development and testing of a field  
81 deployable system called the Soil Water Isotope Storage System (SWISS). The SWISS was built  
82 to be paired with ACCURELL PP V8/2HF vapor permeable probes that have been previously  
83 tested for soil water isotope applications (Rothfuss et al., 2013; Oerter et al., 2017). Our system  
84 uses three basic components to store water vapor produced by the vapor permeable probes: glass  
85 flasks, stainless steel tubing and a flask selector valve (Fig. 1, Supplemental Table 1).  
86 Previously, we demonstrated through a series of lab experiments that the glass flasks used in the

87 SWISS units can reliably store water vapor for up to 30 days (Havranek et al., 2020). That proof-  
88 of-concept study demonstrated that the flasks retain original water isotope values, but the  
89 laboratory system was not field deployable and did not have customizable automation. Here, we  
90 present a fully autonomous, field-ready system that has been tested under both laboratory  
91 conditions and field conditions, including development and testing of a solar-powered, battery  
92 backed automation system that enables pre-scheduled water vapor sampling without manual  
93 intervention in remote field locations.

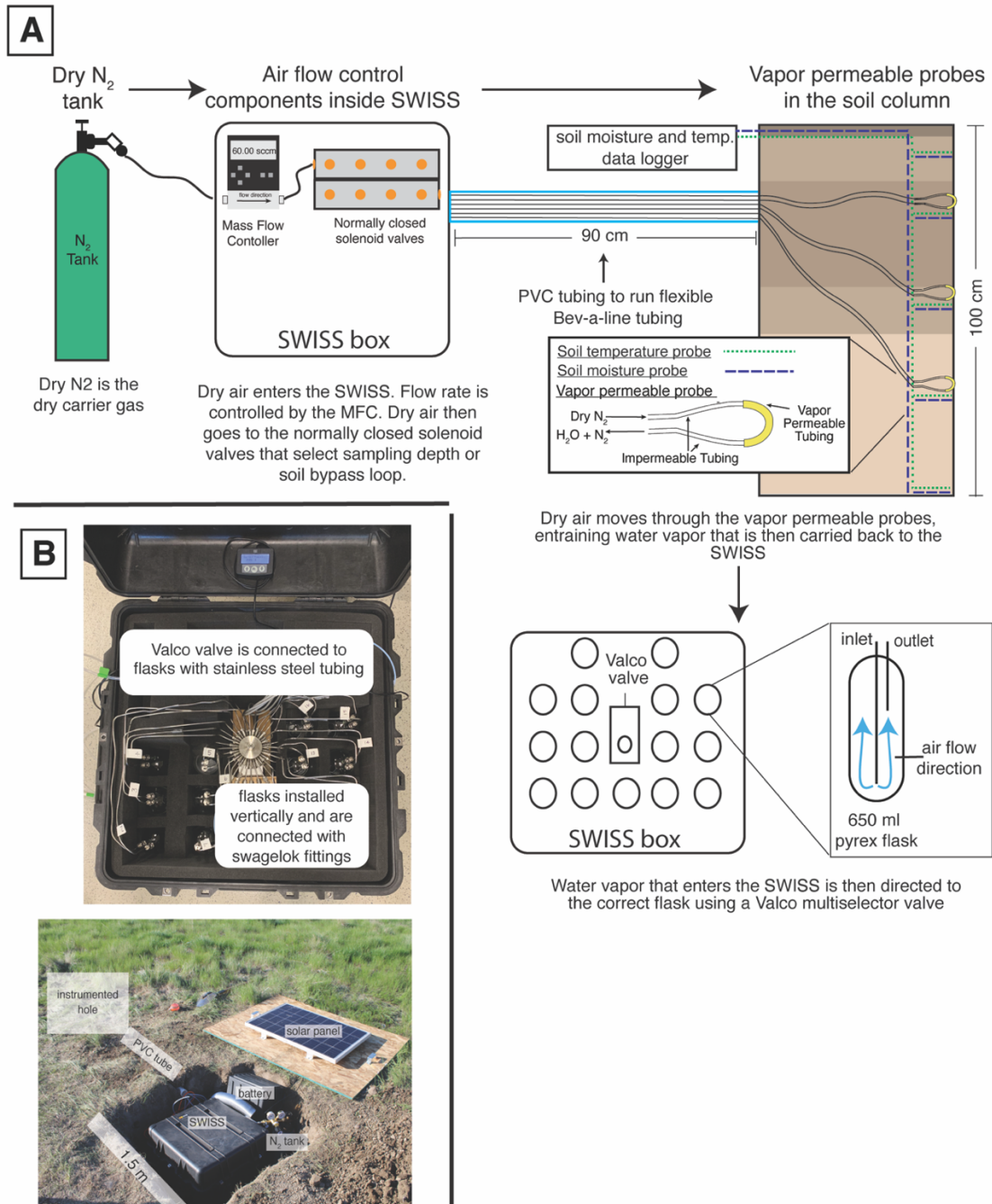
94 To test the accuracy and precision of the SWISS, we completed quality assurance and  
95 quality control (QA/QC) tests. Here, we demonstrate the viability of this system under field-  
96 conditions through two field suitability experiments. In addition, we sampled three different field  
97 sites to show that the automation schema works on a monthly timescale and that the system  
98 preserves soil water vapor isotope signals with sufficient precision to distinguish between three  
99 different field settings and vertical profile differences.

## 100 **2 Field Sites**

### 101 ***2.1 Site Set-Up***

102 At each site we dug two holes; figure 1 shows the field-setup employed at all of our field  
103 sites. One hole was instrumented with soil moisture and temperature data loggers at 25 cm, 50  
104 cm, 75 cm, and 100 cm depths, as well as the water vapor permeable probes at 25 cm, 50 cm and  
105 75 cm depths (Fig 1A). We deployed all probes >9 months before the first samples were  
106 collected to allow the soil to settle and return to natural conditions as much as possible. This  
107 timeframe was longer than other studies (e.g. Kübert et al., 2020) and included infiltration of  
108 spring and early summer precipitation. During probe deployment we took care to retain the  
109 original soil horizon sequence and horizon depths as much as possible. In the second hole, we  
110 stored the SWISS unit, dry nitrogen tank, and associated components to power the SWISS (Fig  
111 1B). The water vapor probes, which connected to the SWISS units with Bev-A-Line  
112 impermeable tubing, were run through a PVC pipe buried at approximately 15 cm depth. We ran  
113 the impermeable tubing underground to limit the effect of diurnal temperature variability on the  
114 impermeable tubing to prevent condensation as water travels from the relatively warm soil to the  
115 SWISS.

116



117  
 118 **Figure 1.** A) The sampling flow path. To sample soil water, dry nitrogen is regulated at a specific rate  
 119 using a mass flow controller, and then directed to one of the three sampling depths, or the soil bypass loop  
 120 using a set of solenoid valves. Both the mass flow controller and solenoid valves are housed inside the  
 121 SWISS. Once directed to the correct sampling depth, dry nitrogen is carried to the vapor permeable  
 122 probes via gas impermeable tubing that is buried approximately 15 cm depth. After passing through the  
 123 vapor permeable probe, the entrained soil water vapor is carried back to the SWISS where it is directed to  
 124 the correct flask using a Valco multiselector valve. B) Photos of a built-out SWISS and the layout of a  
 125 field site. Each of the system components (solar panel, battery,  $N_2$  tank, SWISS, PVC tube) are labeled, in  
 126 addition to the location of the instrumented hole in which all of the probes are buried. The hole which  
 127 houses the SWISS, power, and  $N_2$  tank is approximately 1.5 m wide.

## 128 **2.2 Site descriptions**

129 We deployed the SWISS at three field locations: Oglala National Grassland, Nebraska,  
130 USA; Briggsdale, Colorado, USA; and Seibert, Colorado, USA. The Oglala National Grassland  
131 site (Lat: 42.9600/Long: -103.5979/Elev: 1117 m) is located in northwestern Nebraska, USA in a  
132 cold semi-arid climate. The soil at this site is described as an Aridisol with a silt-loam texture. It  
133 is part of the Olney series (Natural Resources Conservation Service, 2022). The Briggsdale site  
134 (Lat: 40.5947/Long: -104.3190/Elev: 1480 m) is located in northeastern Colorado, USA in a cold  
135 semi-arid climate. The soil at this site is described as an Alfisol with a loamy sand - sandy loam  
136 texture. It is part of the Olnest series (Natural Resources Conservation Service, 2022). Long term  
137 meteorological data from the Briggsdale site is available from the co-located CoAgMet site  
138 (CoAgMet, Colorado Climate Center). The Seibert site (Lat: 39.1187/Long: -102.9250/Elev:  
139 1479 m) is located in eastern Colorado, USA in a cold semi-arid climate. The soil at this site has  
140 been described as an Alfisol, that has a sand loam texture in the top 50 cm of the profile, and a  
141 silt loam texture between 50 - 100 cm. It is part of the Stoneham series (Natural Resources  
142 Conservation Service, 2022). Long term meteorological data from the site is available from the  
143 co-located CoAgMet site (CoAgMet, Colorado Climate Center).

## 144 **3 Materials**

### 145 **3.1 SWISS Hardware components**

146 In each SWISS there are 15 custom made ~650 ml flasks. These flasks are designed  
147 similarly to those used for other water vapor applications. For example, a similar flask is  
148 currently used in an unmanned aerial vehicle to collect atmospheric water vapor samples for  
149 stable isotope analysis (Rozmiarek et al., 2021). The flasks have one long inlet tube that extends  
150 into the flask almost to the base, and one shorter outlet tube so that vapor exiting the flask is well  
151 mixed and representative of the whole flask (Fig. 1A). The large flask volume is advantageous  
152 because there is a low glass surface area to volume ratio, and therefore we are able to reliably  
153 measure vapor from the flasks on a cavity ring down spectroscopy (CRDS) instrument without  
154 interacting with vapor bound to the flask walls. The 15 glass flasks are connected to a 16-port,  
155 multi-selector Valco valve. We chose to use a Valco valve because these have previously been  
156 shown to sufficiently seal off sample volumes for subsequent stable isotope analysis (Theis et al.,  
157 2004). The valve and flasks are connected by 1/8 inch stainless steel tubing and stainless steel  
158 1/4 inch to 1/8 inch union Swagelok fittings; we use PTFE ferrules on the glass flasks with the  
159 Swagelok fittings. The first port of the Valco valve is 1/8 inch stainless steel tubing that serves as  
160 a flask bypass loop, which enables flushing of either dry air or water vapor through the system  
161 without interacting with a flask. All components are contained in a 61 cm x 61 cm x 61 cm  
162 Pelican case (Pelican 0370) with three layers of Pick n' Pluck foam and convoluted foam  
163 (Pelican Products Inc., Torrance, Ca, USA). This case is thermally insulated and provides  
164 enough protection to safely transport the SWISS by vehicle to field sites.

### 166 **3.2 Soil Probes**

167 There are three components for the collection and analysis of soil water vapor: vapor  
168 permeable probes, soil temperature loggers, and soil moisture sensors (Fig 1B, Supplemental  
169 Table 1).

170 Here, we use a vapor permeable membrane (Accurell PP V8/2HF, 3M, Germany) that  
171 was first tested for soil water isotope applications by Rothfuss et al., (2013). This method works  
172 by flushing dry nitrogen (or dry air) through the vapor permeable membrane, creating a water

173 vapor concentration gradient from inside the probe to the soil, thus inducing water vapor  
174 movement across the membrane. Water vapor is then entrained in the dry nitrogen and flushed to  
175 either a CRDS system or into a storage container. We opted to use this tubing because it has been  
176 shown to deliver reliable data over time (i.e. Rothfuss et al., 2015; Oerter et al., 2019; Kübert et  
177 al., 2020; Seeger and Weiler, 2021; Gessler et al., 2021), and it is easy to use and customize to  
178 individual needs (Beyer et al., 2020; Kübert et al., 2020). We previously observed that variability  
179 in the length of the vapor permeable tubing can lead to systematic offsets in the stable isotope  
180 composition of measured waters that arise from variability of vapor permeable tube surface area  
181 (Havranek et al., 2020). Therefore, we were careful to construct all probes such that the length  
182 of the Accurrell vapor permeable tubing was 10 cm long, and the impermeable Bev-A-Line IV  
183 connected on each side of the vapor permeable tubing was 2 m long. We cut the Bev-A-Line  
184 connections to identical lengths to control for memory effect and to treat all samples identically.  
185 We also constructed the vapor permeable probes to be used in the lab setting for standards in an  
186 identical fashion.

187 Soil temperature loggers (Onset HOBO MX2201), used for applying a temperature  
188 correction to all soil water vapor data and to provide key physical parameters of the soils for  
189 other goals beyond this study, were buried at the same depths as the vapor permeable probes.  
190 Soil moisture sensors (Onset S-SMD-M005) were also buried at the same depths as the vapor  
191 permeable probes.

192

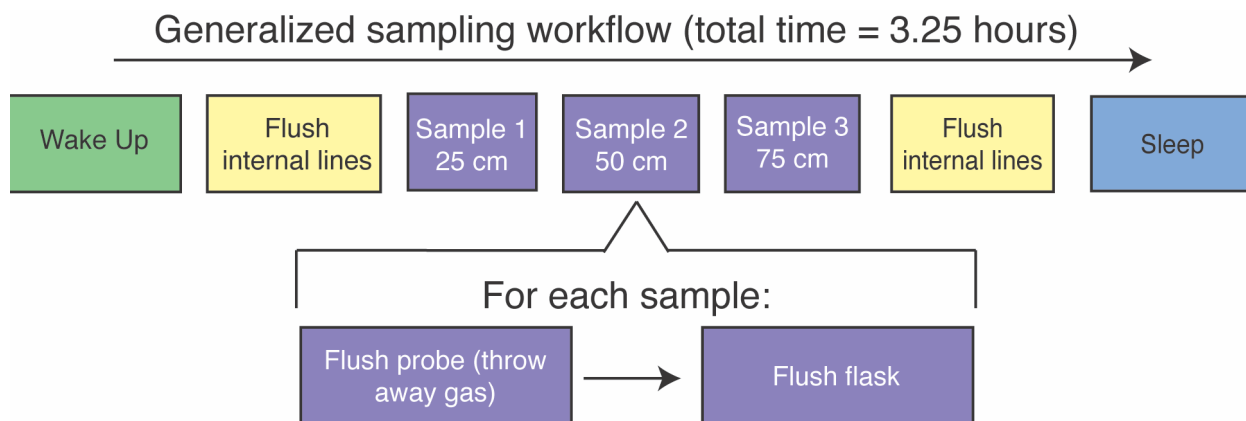
### 193 **3. 3 Automation components, code style, and remote setting power**

194 The philosophy behind the automation of the SWISS was to make it as easy to reproduce  
195 as possible, and as flexible as possible to meet different users' sampling needs. We therefore use  
196 widely available hardware components and electronics parts; for each product there are  
197 numerous alternatives which should be equally viable and could be swapped to better meet each  
198 user's needs. In an effort to make our system as accessible and customizable as possible for the  
199 scientific community, all automation code is completely open source and will continue to be  
200 refined for future applications and hardware improvements. We note that all code is provided as-  
201 is and should be tested carefully for use in other experiments.

202 The overall sampling scheme used in this paper is described in figure 2 and table 1. Our  
203 experimental goal was to create a time series of soil water vapor data from three discrete  
204 sampling depths (25 cm, 50 cm, 75 cm). Prior to sampling any soil water vapor, we bypassed the  
205 soil probes and flushed the lines within the SWISS. Then, at the start of sampling for each depth,  
206 we also flushed the water vapor probe to remove condensation or 'old' water vapor. The gas  
207 from both of those steps was expelled via the flask bypass loop. Each soil depth was then  
208 sampled for 45 minutes by flushing through the next flask designated in the sequence.

209 Supplemental figure 1 shows the components of the automation system. To automate and  
210 program the sampling scheme, we used: (1) a microcontroller to run the automation script; (2) a  
211 coin-cell battery powered real time clock so that the microcontroller was always capable of  
212 keeping track of time through power losses, and therefore maintain the sampling schedule; (3) an  
213 RS-232 to TTL converter for serial communication with the Valco valve; (4) solenoid valves that  
214 were used to control which depth was being sampled and the associated direct current (VDC)  
215 power relay; (5) a mass flow controller used to control the rate at which dry nitrogen (1 ppm  
216 H<sub>2</sub>O) is flushed through the probes; and (6) a power relay used to power the Valco valve and  
217 mass flow controller. All parts are described in detail in Supplemental Table 2.

218



219  
220 **Figure 2.** Flow chart of the instrument schedule used for sampling during all field experiments.  
221

222 **Table 1.** Description of soil water sampling steps

Code Step	Wake-up	Flush internal lines	Flush depth 1	Sample depth 1	Flush depth 2	Sample depth 2	Flush depth 3	Sample depth 3	Flush internal lines	sleep
time (minutes)	1	15	10	45	10	45	10	45	15	1
Valco valve position	flask bypass	flask bypass	flask bypass	2, 5, 8, 11, or 14	flask bypass	3, 6, 9, 12, or 15	flask bypass	4, 7, 10, 13, or 16	flask bypass	flask bypass
solenoid valve position	none	soil bypass	25 cm	25 cm	50 cm	50 cm	75 cm	75 cm	soil bypass	none

223  
224 In a remote setting, the SWISS units are powered using the combination of a 12 volt  
225 deep-cycle battery with a 12VDC, 100 watt solar panel that is used to charge the battery. The  
226 solar panel is mounted to a piece of plywood that covers the hole where the SWISS is deployed  
227 (note, the hole is uncovered in Fig. 1B for illustrative purposes). We opted for this setup because  
228 the underground storage of all parts of the system creates a discreet field site that attracts  
229 minimal attention from other land users, and helps reduce exposure to temperature and  
230 precipitation extremes. In the field, we used a 12VDC-120VAC power inverter to provide simple  
231 plug and play power for the Valco valve and mass flow controller. This simple combination was  
232 suitable for summertime in the Western U.S. where there are many hours of direct sunlight, and  
233 the solar panel was able to easily charge the 12V battery. This setup may need to be adjusted  
234 based on location and desired sampling time. Like the automation system, there are many  
235 commercial options available for products, and they can be easily adjusted for users' needs;  
236 example parts are described in detail in Supplemental Table 2. We also note that in areas where it  
237 is possible to plug into a power grid, the deep cycle battery, solar panel and power inverter can  
238 be removed.

## 239 **4. Methods**

240 We completed all water vapor isotope analyses in the Stable Isotope Lab at the Institute  
241 of Arctic and Alpine Research (INSTAAR SIL) at the University of Colorado Boulder between  
242 October 2020 and August 2022. We used a Picarro L-2130i water isotope analyzer (Picarro, Inc.  
243 Santa Clara, CA) to measure both water concentration and the oxygen and hydrogen isotope  
244 ratios of the water vapor.

### 245 246 **4.1 QA/QC: Testing the SWISS under lab conditions**

247 Our highest order concern for the SWISS is that it remains leak-free, because leaks would  
248 introduce the potential for fractionation or mixing of atmosphere that would alter the stable  
249 isotope ratio of the water vapor in the flask. To mitigate leaks, we developed a three-part quality  
250 assurance and quality control (QA/QC) procedure that must be completed for each new SWISS  
251 prior to the first deployment. The first step detects any large, fast leaks using helium detection  
252 methods; the second step detects medium scale leaks using dry air; and the third step detects  
253 slow, small scale leaks using water vapor tests. Full procedural descriptions are available in the  
254 supplemental material and the data processing code is available via GitHub.

#### 255 256 **4.1.1 Step 1: Use helium to detect large, fast leaks**

257 After initial assembly of the SWISS units, we looked for large leaks from the cracking of  
258 inlet or outlet tubes on the glass flasks that occasionally occurred while tightening the Swagelok  
259 fittings. To do this, we filled the flasks with helium and used a helium leak detector (Leak  
260 Detector, Catalog #22655, Restek, Bellefonte, PA, USA). Another easy alternative to a helium  
261 leak test is to complete a very short dry air test (methods described below) where the hold-time is  
262 on the order of 12-24 hours.

#### 263 264 **4.1.2 Step 2: Use dry air to detect medium scale leaks**

265 The goal of this test was to catch any second order, medium-scale leaks associated with  
266 either Valco valve fittings or Swagelok fittings that were under tightened.

##### 267 268 *Step 2A: Fill flasks with dry air*

269 To start every experiment, we filled flasks with air that is filtered through Drierite (which  
270 has a water vapor mole fraction of less than 500 ppm), at 2 L/min for 5 minutes. With a flask  
271 volume of 650 ml, this means the volume of the flask is turned over 15 times.

##### 272 273 *Step 2B: Hold period*

274 Flasks were then sealed and left to sit for seven days. This time period can be adjusted by  
275 other users to fit their climate or needs.

##### 276 277 *Step 2C: Measure water vapor mole fraction using dead-end pull sample introduction*

278 At the end of the seven-day period, we measured each flask using a dead-end pull sample  
279 introduction method. For this sample introduction method, the inlet to the Valco valve was  
280 sealed with a 1/4 inch Swagelok cap and there was no introduction of a carrier gas. As a result,  
281 air was removed from the flask based on the flow rate of the Picarro analyzer (typically 27 - 31  
282 ml/min). Flasks were measured for five minutes, which resulted in ~150 ml of air being removed  
283 from the flasks. All components within the SWISS are capable of being fully evacuated. Water  
284 vapor mole fractions determined by Picarro instruments are not standardized, so it is impossible



285 to know for sure the exact magnitude of water vapor mole fraction change between the input  
286 analysis and the final value at the end of the dry air test. However, these instruments are  
287 remarkably stable over weeks, and so the relative changes observed (e.g. increase or decrease of  
288 mole fraction relative to the initial amount) are likely reliable, particularly for the larger  
289 magnitude changes.

290 If a flask had a water vapor mole fraction of less than 500 ppm, it “passed” step 2 of  
291 QA/QC. If a flask had a water vapor mole fraction greater than 500 ppm, it “failed” step 2 of  
292 QA/QC, and we tightened both the Swagelok connections on the flasks as well as the fittings  
293 between the stainless steel tubing and the Valco valve. We repeated dry air tests on any given  
294 SWISS unit until the majority (typically at least 13/15) of the flasks had passed step 2 of QA/QC.  
295

#### 296 **4.1.3 Step 3: Water vapor tests detect small scale leaks**

297 The purpose of this experiment was to mimic storage of water vapor at concentrations  
298 similar to what we might expect in a soil, and for durations similar to those of our field  
299 experiments. These experiments were meant to test whether flasks filled early in the sampling  
300 sequence during field deployments leak by the time samples are returned to the lab for  
301 measurement. For this experiment, we filled flasks with water vapor of known isotopic  
302 composition and water vapor mole fraction, sealed the flasks for 14 days, and then measured the  
303 water vapor mole fraction and isotope values of each flask. We performed 11 water vapor tests  
304 that were done across three analytical sessions using six different SWISS units. Across these  
305 three sessions, we measured 164 flasks both at the start of the 14-day experiment, and at the end.  
306

##### 307 *Step 3A: Flush flasks with dry air*

308 Prior to putting any water vapor into the flasks (either in the field or in the lab), we  
309 completed a dry air fill (as described in QA/QC step 2A) that served to purge the flasks of any  
310 prior water vapor that might exchange with the new sample.  
311

##### 312 *Step 3B: Fill flasks with water vapor and measure input isotope values*

313 To supply water vapor to the flasks, we used the vapor permeable probes that were  
314 constructed identically to those deployed in the field. We immersed the probes up to the  
315 connection between the vapor permeable and impermeable tubing in water, taking care to not  
316 submerge the connection point and inadvertently allow liquid water to enter the inside of the  
317 vapor permeable tubing. We flushed the flasks at a rate of 150 ml/min for 30 minutes, and  
318 measured the  $\delta^{18}\text{O}$  and  $\delta^2\text{H}$  values and mole fraction of water vapor as each flask was filled. To  
319 fill 15 flasks sequentially, the probes were submerged in water for approximately 7.5 hours.

320 Across three different sessions, we used three different waters that are tertiary standards  
321 in the INSTAAR SIL to complete these experiments: a light water made from melting and  
322 filtering Rocky Mountain snow ( $\sim -25.5\text{‰}$  and  $-187.5\text{‰}$  VSMOW, for  $\delta^{18}\text{O}$  and  $\delta^2\text{H}$ ,  
323 respectively), an intermediate water that is deionized (DI) water from the University of Colorado  
324 Boulder Campus ( $\sim -16.2\text{‰}$  and  $-120.7\text{‰}$  VSMOW for  $\delta^{18}\text{O}$  and  $\delta^2\text{H}$ , respectively) and a heavy  
325 water that is filtered water sourced from Florida, USA ( $\sim -0.8\text{‰}$  and  $-2.8\text{‰}$  VSMOW for  $\delta^{18}\text{O}$   
326 and  $\delta^2\text{H}$ , respectively). All tertiary lab standards are characterized relative to international  
327 primary standards obtained from the International Atomic Energy Agency and are reported  
328 relative to the VSMOW/SLAP standard isotope scale. To calculate the input value, we averaged  
329  $\delta^{18}\text{O}$  and  $\delta^2\text{H}$  values over the last three minutes of the filling period. We then stored the water

330 vapor in the flasks for 14 days. At the end of the 14-day storage period, we measured each flask  
331 to evaluate if the  $\delta^{18}\text{O}$  and  $\delta^2\text{H}$  values had significantly changed over the storage period.

332

### 333 *Step 3C: Measure the water vapor isotope values*

334 To mitigate memory effects between flasks, we ran dry air via the flask bypass loop (port  
335 one of every SWISS unit) for five minutes between each flask measurement. To verify that the  
336 impermeable tubing between the SWISS and the Picarro instrument was sufficiently dried, we  
337 waited until the water vapor mixing ratio being measured by the Picarro instrument was below  
338 500 ppm for >30 seconds.

339 During this five-minute window, we used a heat gun to manually warm each flask. We  
340 believe heating the flasks creates a more stable measurement by limiting water vapor bound to  
341 the glass walls of the flask and by helping to homogenize the water vapor within the flask. While  
342 we did not strictly control or regulate the temperature of the flasks, they were all warm to the  
343 touch.

344 Once we warmed the flask and dried the impermeable tubing, water vapor was introduced  
345 to the CRDS using one of two methods: 1) the dead-end pull sample introduction method  
346 described above, or 2) a *dry air carrier gas sample introduction* method. During the dry air  
347 carrier gas sample introduction method, dry air is continuously flowing through the flask at a rate  
348 of 27-31 ml/min for the entire 12-minute measurement period. To reach a water vapor mole  
349 fraction of approximately 25,000 ppm (the optimal humidity range for the Picarro L2130-*i*), we  
350 diluted the water vapor with dry air at a rate of 10 ml/min. Without dilution, the concentration  
351 out of the flasks is as high as 35,000 - 40,000 ppm, which leads to linearity effects on a Picarro  
352 L2130-*i* that can be challenging to correct for. The dead-end pull method is preferable when the  
353 water vapor mole fraction inside the flask is low (<17,000 ppm), because there is no additional  
354 introduction of dry air. The introduction of dry air decreases the water vapor mole fraction  
355 throughout the measurement, and in fairly dry flasks, using the dry air carrier gas method can  
356 lower the water vapor mole fraction to below 10,000 ppm. Below 10,000 ppm, there are large  
357 linearity isotope effects associated with the measurement on a Picarro L2130-*i*, and the isotope  
358 values are challenging to correct into a known reference frame, just as with high water vapor  
359 mole fractions. The major downside of the dead-end pull method is that condensation is more  
360 likely to form in the stainless-steel tubing that connects the flasks to the Valco valve, as well as  
361 the Valco valve itself, compared to the dry air carrier gas method. The dry air carrier gas method  
362 prevents condensation from forming in the Valco valve and tubing, and prevents fractionation  
363 that may occur because of changing pressure within the flask. It is possible that during a dead-  
364 end pull on the flask, heavier isotopes may remain attached to the walls of the flask, coming off  
365 later as the pressure drops. For these reasons, the dry air carrier gas sample introduction method  
366 is our preferred method for sample introduction in most cases.

367 For each flask, we looked at the stability of the isotope values as well as either a stable  
368 water vapor mole fraction if the dead end pull method was being used or a steady, linear decrease  
369 in water vapor mole fraction if the dry air carrier gas method was being used. For approximately  
370 90% of the flasks we found that after excluding the first three minutes of measurement of each  
371 flask, the subsequent three minutes were the most stable. For the remaining ~10% of the flasks,  
372 using a time window that started either ~30 seconds earlier or ~30 seconds later to create an  
373 average isotope value offered a more stable isotope signal with smaller instrumental  
374 uncertainties. Any flask that required specialized treatment during the data reduction process was  
375 flagged during measurement.

376

377 *Step 3D: Data correction*

378 During these experiments, we monitored instrument performance (e.g. drift) in two ways.  
379 First, to run standards identically to how samples were collected, we introduced tertiary  
380 standards, described above, using vapor probes. The water vapor produced by the vapor  
381 permeable probes was flushed through the SWISS unit via the flask bypass loop and diluted with  
382 a 10 ml/min dry air flow to reach a water vapor mole fraction of approximately 25,000 ppm  
383 before entering the Picarro instrument. Second, we introduced a suite of four secondary  
384 standards that have been calibrated against primary standards, and reported against  
385 VSMOW/SLAP via a flash evaporator system described in detail by Rozmiarek and others  
386 (2021). This flash evaporator system can be used to adjust the water vapor mole fraction to  
387 create linearity corrections at high and low water vapor mole fractions. After correcting data into  
388 a common reference frame, we calculated the difference between the input isotope values and the  
389 ending isotope values.

390 The results of these tests were used to carefully document flasks that do not perform well,  
391 and any idiosyncrasies of SWISS units. That way, during field deployment suspicious flasks  
392 could be easily identified and investigated.

393

394 **4.2 Field suitability experiments:**

395 ***4.2.1 Field suitability experiment #1: Long term field dry air test***

396 As a complement to the QA/QC we did under lab conditions, we also completed long  
397 term dry air tests at our field sites. We had three goals associated with these experiments. The  
398 first was to test whether, even under field conditions, where daily temperature and relative  
399 humidity fluctuations are different than in a lab setting, the flasks were still resistant to  
400 atmospheric intrusion. Second, we used these tests to evaluate whether the flasks that were  
401 flushed with soil water vapor near the end of a sampling sequence took on atmosphere prior to  
402 sampling. Lastly, we chose these time intervals because they bracket the typical length of a  
403 deployment, which helped us determine how quickly flasks should be measured after bringing a  
404 SWISS back to the lab.

405 Like all field deployments, we started with a dry air fill, and then one SWISS unit was  
406 deployed to each of our three field sites. No soil water was collected during these deployments.  
407 The duration between filling the flasks with dry air to measuring the flasks was between 34 - 52  
408 days. The 34 and 52 day tests were done during June 2022 and August 2021, respectively, and  
409 therefore tests the SWISS under warm summertime conditions. The 43 day test was done in  
410 October 2021, which included nights where air temperatures fell below 0°C. The only barrier  
411 between air and the SWISS in its deployment hole was a plywood board, and so this deployment  
412 tested the suitability of the SWISS to maintain integrity under freezing conditions.

413

414 ***4.2.2. Field suitability experiment #2: Mock field tests***

415 To test whether the automation code and sampling scheme we developed worked as  
416 expected on short, observable timescales, we set up an experiment to simulate field deployment  
417 of one SWISS unit (Meringue) near the University of Colorado Boulder. This test applied the  
418 automation components and remote power setup described in the materials section. During this  
419 field-simulation experiment, our goal was to collect three discrete samples each sampling period,  
420 to simulate the collection of water vapor from three soil depths. An important goal of this test

421 was to test whether the sampling scheme introduced any memory effects between samples. We  
422 followed the sampling protocol described in figure 2 and table 1.

423 The day before the experiment began, all flasks were flushed with dry air as described in section  
424 4.1.2. Over the course of 25 hours, all 15 flasks were filled with three different vapors according  
425 to a set schedule as would be done in the field. Two of the vapors were created by immersing the  
426 water vapor permeable probes in the light water and intermediate water as described in section  
427 4.1.3. The third was water vapor from the ambient atmosphere. All three vapors were sampled  
428 using vapor permeable probes constructed identically to those deployed in the field. For this  
429 experiment, we filled three flasks per cycle with each one of the waters (e.g. Flask 2 = light,  
430 Flask 3 = intermediate, Flask 4 = atmosphere). The choice to sample atmosphere alongside two  
431 waters reflects our second goal of this test, which was to demonstrate that sampled water vapor  
432 isotope values do not drift towards atmospheric values (Magh et al., 2022).

433 Following the sampling schedule, we stored the SWISS unit in a simulated field setting  
434 for seven days. At the end of the seven days, we measured the flasks. For flasks that had a high  
435 water vapor mole fraction (i.e. light and intermediate water vapor samples) we used the dry air  
436 carrier gas sample introduction method. For flasks that had a low water vapor mole fraction (i.e.  
437 atmosphere, ~15,000 ppm) we used the dead end pull sample introduction method.

438 To create average values for each flask, we followed the same averaging protocol  
439 described in section 4.1.3. We used equations 2A and 2B from Rothfuss et al., (2013) to convert  
440 from water vapor to liquid values. Then, using secondary and tertiary standards, data were  
441 corrected into the VSMOW/SLAP isotope scale. Finally, the SWISS unit offset correction  
442 (detailed below in section 6.1.2) was applied.

#### 443 444 **4.3 Example Field Deployment: One month period**

445 We deployed one SWISS unit each to the three field sites described in summer 2022.  
446 Before deployment, all SWISS units were flushed with dry air following the protocol outlined in  
447 section 4.1.2. Flasks were flushed with dry air one to three days prior to field deployment. At  
448 each site, we sampled at three depths (25 cm, 50 cm, and 75cm) on each sampling day, following  
449 the protocol described in figure 2 and table 1. We sampled soil water from all three depths every  
450 five days (protocol length = 25 days total). At Oglala National Grassland, samples were taken  
451 every five days from 2022-06-25 to 2022-07-14. At the Briggsdale, CO site samples were taken  
452 every five days between 2022-07-17 and 2022-08-06. At the Seibert, CO site, samples were  
453 collected every five days between 2022-06-19 and 2022-07-04. At the end of a 28-day period,  
454 the SWISS units were returned to the lab, and measured. SWISS units were measured within five  
455 days of returning from the field. The maximum number of days a flask held sample water vapor  
456 during these deployments was 32 days. The measurement protocol and data averaging protocol  
457 follows the procedures described in section 4.1.3. The data correction scheme follows as in the  
458 section 4.2.2.

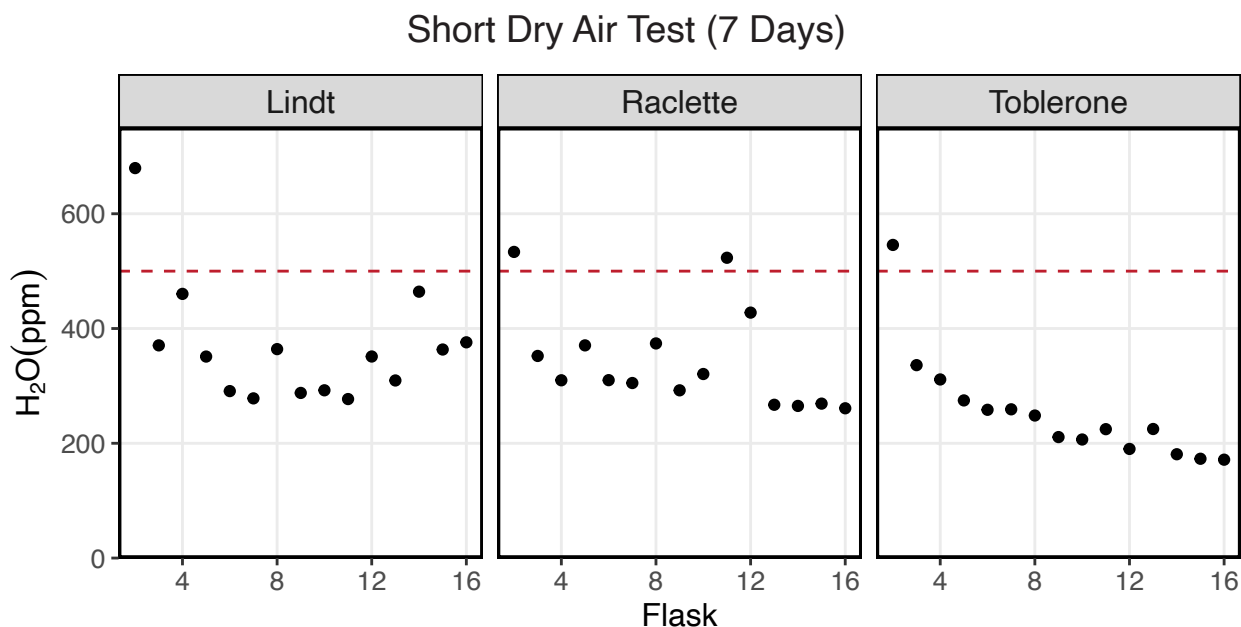
## 459 **5 Results**

### 460 **5.1 QA/QC Results**

#### 461 **5.1.1 Dry air test**

462 Figure 3 shows the results of a seven-day dry air test for three SWISS units (marked by  
463 the unit name) (SI Table 3). For all three SWISS units, at least 13/15 of the flasks maintained a  
464 water vapor mole fraction value of less than 500 ppm over the seven-day period. In two of the

465 three SWISS units (Lindt and Raclette), the water vapor mole fraction for flasks was randomly  
 466 distributed around approximately 350 ppm. In Toblerone there was a systematic decrease in  
 467 water vapor mole fraction from flask two through flask 16, matching the order in which the  
 468 flasks were filled with dry air initially. In all three SWISS units, flask two had the highest water  
 469 vapor mole fraction of all the flasks. Supplemental figure 2 shows the results of successive dry  
 470 air tests on the SWISS unit Toblerone where Swagelok fittings were tightened between tests.  
 471 Between the two tests, there was a significant decrease in measured water vapor mole fraction  
 472 for many flasks, but particularly for flasks 10 and 11 as a result of tightening the fittings.



473  
 474 **Figure 3. Results of a dry air test from three different SWISS units named: Lindt, Raclette and Toblerone. The majority**  
 475 **of the flasks maintain a water vapor mixing ratio of less than 500 ppm.**

476  
 477 **5.1.2. Water vapor test**

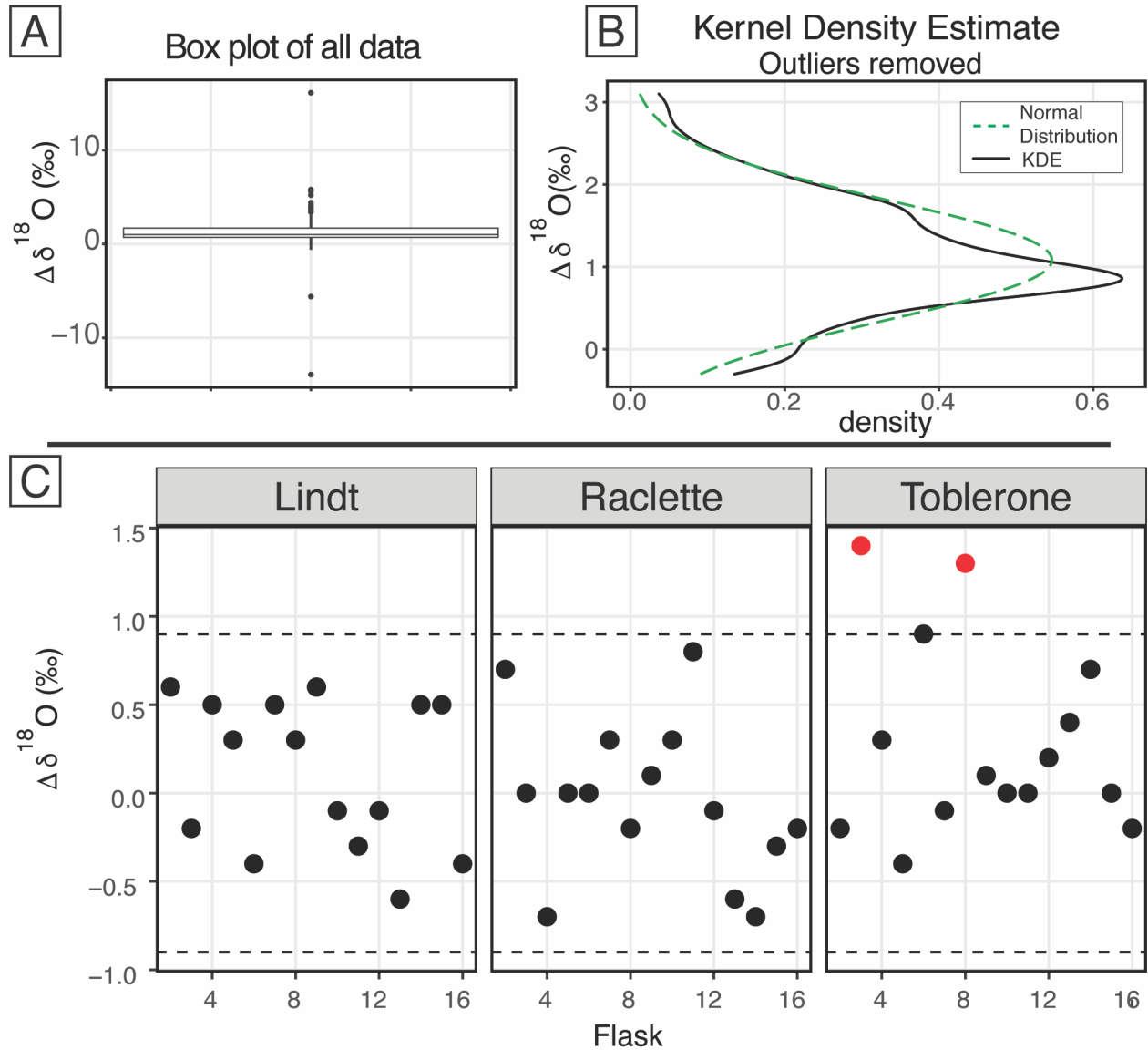
478 Figure 4 shows the  $\delta^{18}\text{O}$  results of 11 water vapor tests performed using six different  
 479 SWISS units. Ideally, we expect a normal distribution centered about 0 within the uncertainty  
 480 limits of the water vapor probes (Oerter et al., 2016). For  $\delta^{18}\text{O}$ , the mean difference between the  
 481 start and end values for the flasks is 1.1‰ with a standard deviation of 0.72‰ (outliers  
 482 removed). There is a consistent positive offset, with a few clear outliers (Fig. 4A). We do not  
 483 observe a consistent difference between water vapor sample introduction methods (Supplemental  
 484 Fig. 3). After removing outliers ( $< Q1 - 1.5 * IQR$  or  $> Q3 + 1.5 * IQR$ ,  $n = 15$ ) from the dataset,  
 485 we compared the kernel density estimate shape to a normal distribution calculated from the mean  
 486 and standard deviation of the dataset to assess dataset normality (Fig. 4B). A normal distribution  
 487 slightly overestimates the center of the data, but captures the overall shape fairly well. Therefore,  
 488 we used the median offset (1.0‰) to correct our water vapor isotope values, and used the  
 489 interquartile range of the dataset (outliers removed) to estimate uncertainty of the SWISS as  $\pm$   
 490 0.9‰. In figure 5C, for simplicity, we just present the results from 45 flasks (three SWISS units),  
 491 with the 1.0‰ offset correction applied. After correction, data are randomly distributed about 0,  
 492 and are within the uncertainty range of  $\pm 0.9‰$  (Supp. Table 4).

493 Figure 5 shows the  $\delta^2\text{H}$  results of 11 water vapor tests. For  $\delta^2\text{H}$ , the mean difference  
 494 between the start and end values is 2.63‰ with a standard deviation of 2.85‰ (outliers

495 removed). Similar to  $\delta^{18}\text{O}$ , we expected a normal distribution of differences centered around 0.  
496 As with  $\delta^{18}\text{O}$ , there was a consistent positive offset with some outliers (i.e.,  $< Q1 - 1.5 \cdot \text{IQR}$  or  $>$   
497  $Q3 + 1.5 \cdot \text{IQR}$ ) (Fig. 5A). After removing outliers ( $n = 26$ ) from the dataset, we compared the  
498 kernel density estimate to a normal distribution calculated from the mean and standard deviation  
499 of the dataset to assess dataset normality (Fig. 5B). As with  $\delta^{18}\text{O}$ , the center of the dataset is  
500 overestimated by the mean, but the overall peak shape is roughly captured. We therefore use the  
501 median value of 2.3‰ as an offset correction and estimate uncertainty at  $\pm 3.7\%$  for  $\delta^2\text{H}$  from the  
502 interquartile range. In figure 5C, we present the results from 45 flasks (three SWISS units), with  
503 the 2.3‰ offset correction applied. Data are randomly distributed about 0 and are within the  
504 uncertainty range of  $\pm 3.7\%$  (Supplemental Table 4).

505 When we compared the results in figures 4C and 5C, we found that flasks that performed  
506 adequately for  $\delta^{18}\text{O}$  did not always perform adequately for  $\delta^2\text{H}$ . The results from the SWISS unit  
507 Lindt display this behavior particularly well. Less commonly, some flasks that were within  
508 uncertainty of the system for  $\delta^2\text{H}$  were not within uncertainty of the system for  $\delta^{18}\text{O}$ , like flask  
509 eight in the SWISS unit Toblerone (Figs. 4C, 5C). In a dual isotope plot, there is a strong  
510 positive correlation between  $\delta^2\text{H}$  and  $\delta^{18}\text{O}$  with a slope of 3.14 and an  $R^2$  value of 0.62  
511 (Supplemental Fig. 4).

512



514

515

516 **Figure 4.**  $\delta^{18}\text{O}$  results of the water vapor tests. A) Boxplot of the difference between the starting  $\delta^{18}\text{O}$ 517 value and the final  $\delta^{18}\text{O}$  value of all 164 flasks. B) After removing the outliers from the dataset, the kernel

518 density estimate (black line) and the normal distribution calculated from the dataset (dashed green) are

519 shown. C) After applying the offset correction of 1.0‰, the difference between the starting  $\delta^{18}\text{O}$  value520 and the final  $\delta^{18}\text{O}$  value for three boxes from the August 2022 session are shown. An uncertainty of  $\pm$ 

521 0.9‰ is marked with a dashed line, and data points that fall outside that uncertainty are colored red.

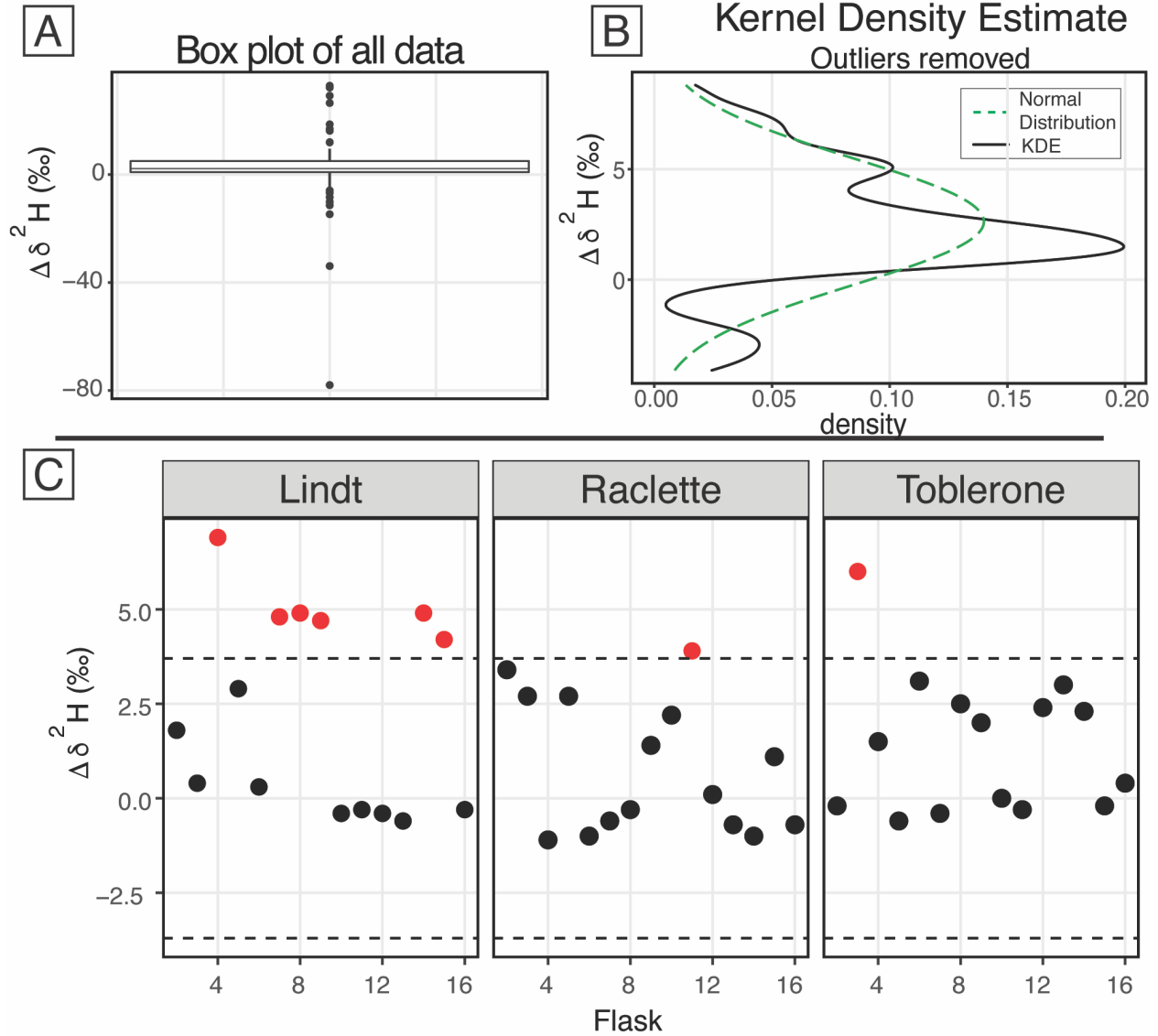
522

523

524

525

526



527  
528  
529  
530  
531  
532  
533  
534

**Figure 5.**  $\delta^2\text{H}$  results of the water vapor tests A) Boxplot of the difference between the starting  $\delta^2\text{H}$  value and the final  $\delta^2\text{H}$  value of all 164 flasks. B) After removing the outliers from the dataset, the kernel density estimate (black line) and the normal distribution calculated from the dataset (dashed green) are shown. C) The difference between the starting  $\delta^2\text{H}$  value and the final  $\delta^2\text{H}$  value for three boxes from the August 2022 session are shown after applying the offset correction of 2.3‰. An uncertainty of  $\pm 3.7\text{‰}$  is marked with a dashed line, and data points that fall outside that uncertainty are colored red.



## 535 **5.2 Field suitability test results**

### 536 **5.2.1 Dry air test**

537 Figure 6A shows the result of placing three different SWISS units that were flushed with  
538 dry air out into the field for 34 - 52 days (SI Table 3). This timescale (four - six weeks) is similar  
539 to most field deployments. At the timescale of 34 - 43 days, 13 of the 15 flasks typically  
540 maintained a water vapor mole fraction of less than 1000 ppm. Over the 52 days, seven flasks  
541 maintained a water vapor mole fraction less than 1000 ppm and the remaining eight had a water  
542 vapor mole fraction between 1000 - 2500 ppm.

543

### 544 **5.2.2 Automation test**

545 Figure 6B shows the results of using the automation code to collect and store water vapor  
546 of known composition for seven days (Table 2). In both plots, the known values of the water are  
547 shown as a long-dash line. Uncertainty on those measurements is estimated at  $\pm 0.5\%$  and  $\pm 2.4\%$   
548 for  $\delta^{18}\text{O}$  and  $\delta^2\text{H}$ , respectively (Oerter et al., 2016), shown as the dotted lines. We estimated the  
549 isotope value of the atmosphere at the time of sampling with water vapor mole fraction,  $\delta^{18}\text{O}$ ,  
550 and  $\delta^2\text{H}$  data from the CRDS in the lab. The isotope value, that was corrected as described in  
551 section 4.2.2, of each flask is shown, with uncertainty associated with the SWISS units estimated  
552 at  $\pm 0.9\%$  and  $\pm 3.7\%$  for  $\delta^{18}\text{O}$  and  $\delta^2\text{H}$ , respectively.

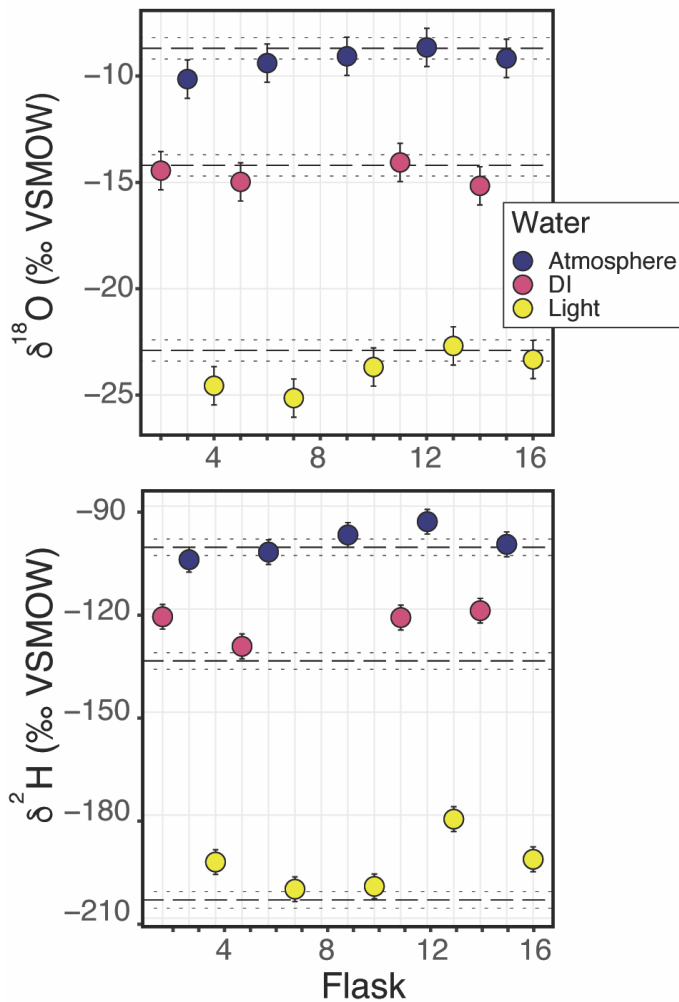
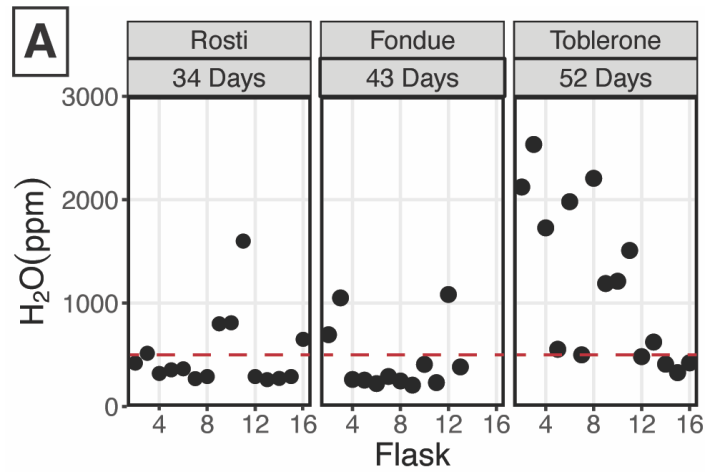
553 Seven of the nine flasks filled with flash-evaporated water vapor overlap within  
554 uncertainty of the known  $\delta^{18}\text{O}$  value for those standards (top plot, Fig. 6B), and four of the five  
555 flasks filled with atmospheric vapor overlap within uncertainty of our estimated  $\delta^{18}\text{O}$  value.  
556 Flasks that fall outside of the bounds of uncertainty have lower  $\delta^{18}\text{O}$  values than the expected  
557 value. For  $\delta^2\text{H}$ , (bottom plot, Fig. 6B) only three of the nine flasks filled with flash-evaporated  
558 water vapor overlap within uncertainty of the known value of those standards, while four of the  
559 five flasks filled with atmospheric vapor overlap within uncertainty of the estimated  $\delta^2\text{H}$  value.  
560 Flasks that fall outside of the bounds of uncertainty have higher  $\delta^2\text{H}$  values than the expected  
561 value.

562

563 **Table 2.** Results of the Automation test

<b>SWISS</b>	<b>Flask</b>	<b>water</b>	<b><math>\delta^{18}\text{O}</math> (‰)</b>	<b><math>\delta^2\text{H}</math> (‰)</b>
Meringue	2	DI	-14.4	-122.2
Meringue	3	Atmosphere	-10.1	-105.6
Meringue	4	Light	-24.6	-193.7
Meringue	5	DI	-15.0	-130.8
Meringue	6	Atmosphere	-9.4	-103.4
Meringue	7	Light	-25.1	-201.5
Meringue	8	DI	-17.3	-140.5
Meringue	9	Atmosphere	-9.1	-98.4
Meringue	10	Light	-23.7	-200.7
Meringue	11	DI	-14.1	-122.5
Meringue	12	Atmosphere	-8.7	-94.5
Meringue	13	Light	-22.7	-181.2
Meringue	14	DI	-15.2	-120.5
Meringue	15	Atmosphere	-9.2	-101.1
Meringue	16	Light	-23.3	-192.9

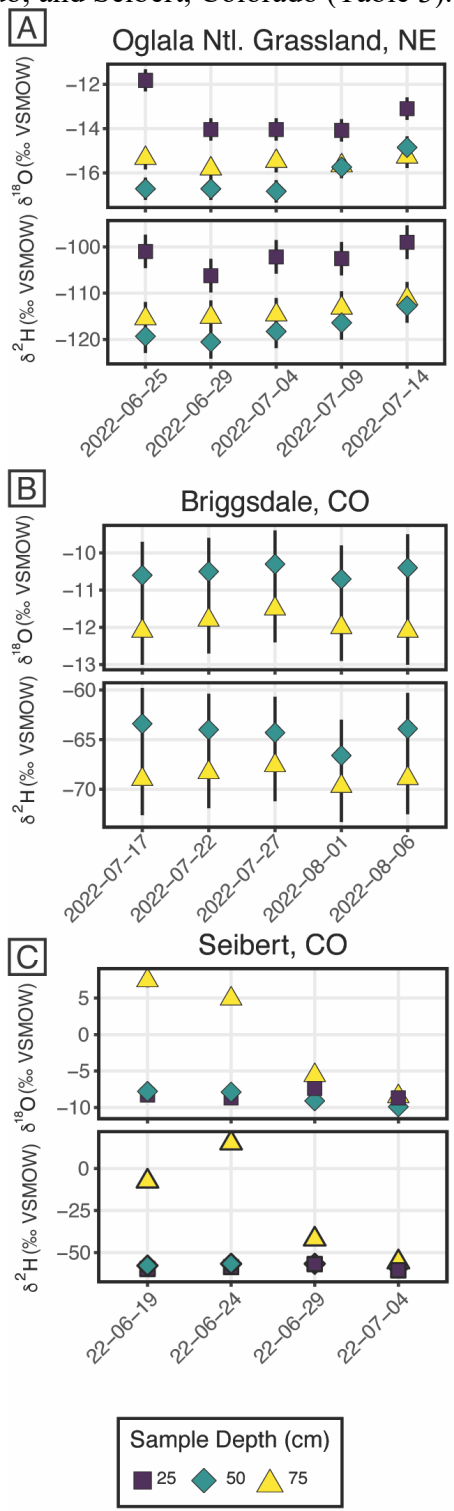
564



565  
 566 **Figure 6.** A) Results from three different field-based long dry air tests. B) Results from the automation  
 567 field suitability tests using the SWISS unit named Meringue. Flasks that sampled atmosphere are shown  
 568 in blue, flasks that sampled deionized water (DI) are shown in pink, and flasks that sampled the light  
 569 water are shown in yellow. The top plot shows the  $\delta^{18}\text{O}$  results, and the bottom plot shows the  $\delta^2\text{H}$  results.  
 570

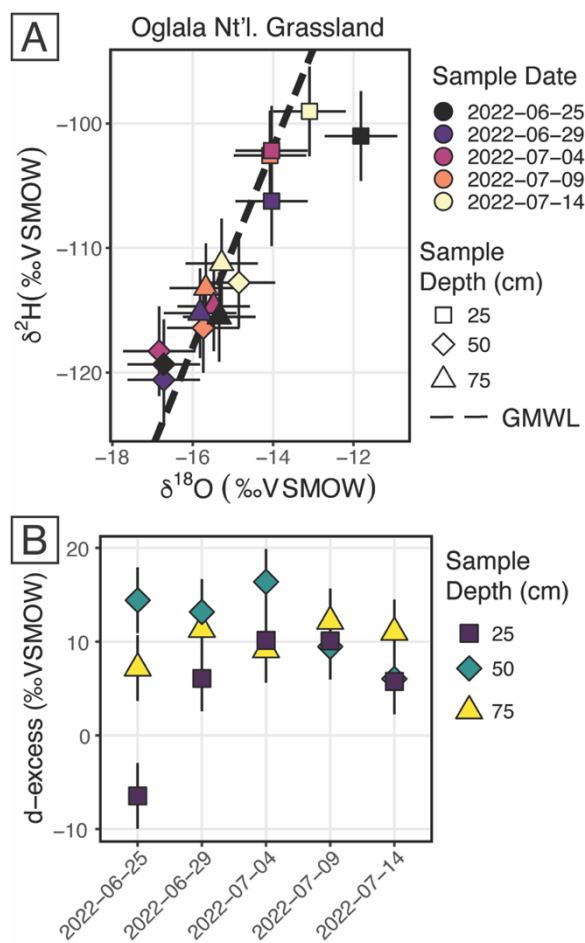
571 **5.3 Example Field deployment results**

572 Figure 7 shows the results from three field deployments in Oglala National Grassland,  
 573 Nebraska; Briggsdale, Colorado; and Seibert, Colorado (Table 3).



574 **Figure 7.** Results from all three field deployments to A) Oglala National Grassland, NE, B) Briggsdale,  
 575 CO and C) Seibert, CO. Note, the y-axis scale for all three plots is different.  
 576

577 There are 15 samples from Oglala National Grassland (Fig. 7A, Table 3); five from 25  
 578 cm depth, five from 50 cm depth and five from 75 cm depth. Four of the five samples from 25  
 579 cm overlap within uncertainty in  $\delta^{18}\text{O}$  value, and all five samples overlap with uncertainty in  $\delta^2\text{H}$   
 580 value. There is a significant decrease in the  $\delta^{18}\text{O}$  value at 25 cm between 2022-06-25 and 2022-  
 581 06-29. There is no similar shift in  $\delta^2\text{H}$  value over the same time period. The first three samples  
 582 from 50 cm overlap in both  $\delta^{18}\text{O}$  and  $\delta^2\text{H}$  values, then the final two samples shift to higher  
 583 isotope values. Similar to the samples from 50 cm, there is a trend towards higher  $\delta^2\text{H}$  values for  
 584 the last three samples. All five samples from 75 cm overlap in  $\delta^{18}\text{O}$  and  $\delta^2\text{H}$  values. On a dual  
 585 isotope plot, data from 50 cm and 75 cm cluster together at lower values, while the  $\delta^{18}\text{O}$  and  $\delta^2\text{H}$   
 586 values from 25 cm are higher (Figs. 7A, 8A). All of the data overlap within uncertainty with the  
 587 global meteoric water line, except for the 25 cm depth sample from 2022-06-25 (Fig. 8A). The  
 588 calculated d-excess values are all within uncertainty of 10‰ ( $\pm 2.6\text{‰}$ ) and of each other between  
 589 2022-06-29 and 2022-07-14 (Fig 8B), except for the 25 cm depth sample from 2022-06-25,  
 590 which has a d-excess value of -6.6‰, typically consistent with evaporative enrichment of soil  
 591 water at that depth and time.  
 592



593 **Figure 8.** Results from the Oglala National Grassland, NE field site. A)  $\delta^2\text{H}$  vs.  $\delta^{18}\text{O}$ , where the dashed  
 594 line is the global meteoric water line. The shapes for the different depths sampled matches figure 7, and  
 595 the color of the points is the date on which the soil water was sampled B) A plot of d-excess. Note, both  
 596 the color and shape match figure 7.  
 597

598           There are 10 samples from Briggsdale, CO (Fig. 7B, Table 3); five samples each from  
599 vapor probes buried at 50 cm and 75 cm depth. Data from 25 cm at Briggsdale, CO were  
600 excluded because the water vapor mole fractions from all of the flasks were extremely low  
601 (<13,000 ppm). We excluded these data because these samples are associated with a very dry  
602 soil (VWC < 0.05), and it is not clear how much sampling gas (N<sub>2</sub>) is injected into the soil using  
603 the vapor permeable tubing under very dry conditions (Quade et al., 2019), and therefore how  
604 representative these isotope data are of soil water. Moreover, below 13,000 ppm there are large  
605 linearity effects on a Picarro L2130-*i*, and it is challenging to correct those data if they were  
606 measured using the dry-air carrier sample introduction method. While all samples overlap within  
607 uncertainty for both  $\delta^{18}\text{O}$  and  $\delta^2\text{H}$  values, the absolute values of samples from 50 cm are  
608 consistently offset to higher values for both  $\delta^{18}\text{O}$  and  $\delta^2\text{H}$  as compared to samples from 75 cm.

609           There are 12 samples from Seibert, CO (Fig. 7C, Table 3); four from each sampling depth  
610 (25, 50 and 75 cm). At 25 cm depth,  $\delta^{18}\text{O}$  values of three of the four samples overlap within  
611 uncertainty, while the 25 cm sample from 2022-06-29 has a higher  $\delta^{18}\text{O}$  value than the other  
612 three samples. At 25 cm depth,  $\delta^2\text{H}$  values overlap within uncertainty for all four samples. At 50  
613 cm depth, there is a steady decrease in  $\delta^{18}\text{O}$  value over the sampling period, while  $\delta^2\text{H}$  values for  
614 all four samples remain steady and overlap within uncertainty. At 75 cm depth, samples have a  
615 very large range of  $\delta^{18}\text{O}$  values between -8.5‰ and 7.4‰, and  $\delta^2\text{H}$  values range between -  
616 55.7‰ and 15.1‰.

617 **Table 3.** Results from the three field deployments of SWISS.

Site	Date	Sample Depth (cm)	Flask	T (°C)	$\delta^{18}\text{O}$ (‰)	$\delta^{18}\text{O}$ (‰) Analytical Error	$\delta^2\text{H}$ (‰)	$\delta^2\text{H}$ (‰) Analytical Error
Briggsdale	2022-07-17	50	3	25.1	-10.8	0.2	-65.6	0.6
Briggsdale	2022-07-17	75	4	23	-12.1	0.2	-69	0.7
Briggsdale	2022-07-22	50	6	25.9	-10.7	0.3	-67.1	0.7
Briggsdale	2022-07-22	75	7	23.6	-11.9	0.2	-69	0.6
Briggsdale	2022-07-27	50	9	24.3	-10.4	0.3	-65.6	0.6
Briggsdale	2022-07-27	75	10	23	-11.5	0.2	-67.6	0.7
Briggsdale	2022-08-01	50	12	23.4	-10.7	0.2	-67	0.7
Briggsdale	2022-08-01	75	13	22.4	-12.0	0.2	-69.1	0.7
Briggsdale	2022-08-06	50	15	24	-10.5	0.2	-65	0.6
Briggsdale	2022-08-06	75	16	22.9	-12.1	0.2	-68.8	0.7
Seibert	2022-06-19	25	2	24.2	-8.3	0.2	-59.8	0.6
Seibert	2022-06-19	50	3	22	-7.8	0.2	-57.8	0.6
Seibert	2022-06-19	75	4	19.4	7.4	0.2	-7.6	0.7
Seibert	2022-06-24	25	5	24	-8.7	0.2	-58.7	0.7
Seibert	2022-06-24	50	6	22.2	-7.9	0.2	-56.7	0.7
Seibert	2022-06-24	75	7	20.5	4.9	0.2	15.1	0.6
Seibert	2022-06-29	25	8	23.2	-7.4	0.2	-56.9	0.6
Seibert	2022-06-29	50	9	21.8	-9.1	0.2	-56.7	0.7
Seibert	2022-06-29	75	10	21	-5.6	0.2	-42.1	0.6
Seibert	2022-07-04	25	11	25	-8.7	0.2	-60.6	0.7
Seibert	2022-07-04	50	12	23.3	-9.9	0.2	-58.8	0.6
Seibert	2022-07-04	75	13	21.5	-8.5	0.2	-55.7	0.7
Oglala Ntl. Grassland	2022-06-25	25	2	23.0	-11.8	0.2	-101	0.7
Oglala Ntl. Grassland	2022-06-25	50	3	22.8	-16.7	0.2	-119.3	0.7
Oglala Ntl. Grassland	2022-06-25	75	4	21.5	-15.3	0.2	-115.5	0.8
Oglala Ntl. Grassland	2022-06-29	25	5	25.0	-14	0.2	-106.2	0.7
Oglala Ntl. Grassland	2022-06-29	50	6	22.8	-16.7	0.2	-120.6	0.7
Oglala Ntl. Grassland	2022-06-29	75	7	21.3	-15.8	0.2	-115.2	0.7
Oglala Ntl. Grassland	2022-07-04	25	8	25.0	-14	0.2	-102.2	0.7
Oglala Ntl. Grassland	2022-07-04	50	9	23.0	-16.8	0.2	-118.3	0.6
Oglala Ntl. Grassland	2022-07-04	75	10	22.0	-15.5	0.2	-114.7	0.6
Oglala Ntl. Grassland	2022-07-09	25	11	23.0	-14.1	0.2	-102.6	0.6
Oglala Ntl. Grassland	2022-07-09	50	12	22.8	-15.7	0.2	-116.4	0.7
Oglala Ntl. Grassland	2022-07-09	75	13	22.0	-15.7	0.2	-113.2	0.6
Oglala Ntl. Grassland	2022-07-14	25	14	23.0	-13.1	0.2	-99	0.6
Oglala Ntl. Grassland	2022-07-14	50	15	22.8	-14.9	0.3	-112.8	0.7
Oglala Ntl. Grassland	2022-07-14	75	16	22.0	-15.3	0.2	-111.2	0.7

618  
619

## 620 6. Discussion

### 621 6.1 QA/QC and field suitability tests

#### 622 6.1.1 Dry Air tests

623 In Colorado, where these tests were completed, the ambient atmosphere during the  
624 summertime typically sits at a water vapor mole fraction between 10,000 - 20,000 ppm, and in  
625 winter the water vapor mole fraction can drop as low as 4000 ppm. If the flasks had been slowly  
626 equilibrating with the atmosphere, the flasks would have drifted to much higher water vapor  
627 molar fractions. If the flasks did not drift towards higher water vapor mole fractions, we felt  
628 confident that the flasks were resistant to atmospheric intrusion after they have been flushed with  
629 dry air. We chose a timescale of seven days for the dry air tests because we found that in a low-  
630 humidity environment, seven days was enough time to meaningfully observe leaks, while being  
631 short enough to work through the QA/QC process efficiently. For example, results of two  
632 sequential dry air tests on the SWISS unit Toblerone (supplemental Fig. 2), show that it is  
633 possible to drastically reduce leaks that allow ambient water vapor from intruding into the flasks  
634 by tightening and/or replacing problematic fittings (both those attached to the glass flasks and  
635 those on the Valco valve) and in some rare cases the glass flask itself. During the final seven-day  
636 dry air tests, most flasks maintained a water vapor mole fraction less than 400 ppm, and all flasks  
637 maintained a water vapor mole fraction of less than 700 ppm (Fig. 3).

638 Across all of the SWISS units, there is a bias towards a higher water vapor mole fraction  
639 for the first flask that is measured (port one on every valve is the flask bypass loop, so the first  
640 flask is flask two), which suggests a methodological source of higher water vapor concentration  
641 rather than Swagelok fitting tightness problems. There are two potential sources for this issue.  
642 First, it is possible that not all of the atmospheric water vapor was flushed from the line that  
643 connects to the CRDS prior to the start of the measurements, but by the time the second flask is  
644 measured, the lines between the SWISS and CRDS have been sufficiently flushed, creating bias  
645 in the first flask measured. This hypothesis could be tested by flushing all of the gas lines with  
646 dry air to progressively lower water vapor mixing ratios prior to measuring any flasks, to see  
647 what minimum ratio is required to eliminate this bias. Lab protocols could then be adjusted to  
648 flush all gas lines to this level. Similarly, it is possible that during the filling phase, not all of the  
649 atmospheric vapor has been flushed out of the Drierite system before starting the fill process.  
650 This hypothesis is supported by the systematic decrease in water vapor mole fraction across  
651 flasks in the Toblerone unit (Fig. 3, right panel). As a result of these biases, we now flush the  
652 Drierite for at minimum 30 minutes prior to the start of the experiment.

653 In addition to testing the leakiness, the dry air test also provided a useful baseline from  
654 which to test building materials. For example, in supplemental figure 5, we show the results of  
655 sequential seven day and 27-day dry air tests where we replaced stainless steel tubing and fittings  
656 with PTFE Swagelok fittings with 1/8 inch PTFE tubing. We thought that PTFE fittings would  
657 be advantageous because they are much easier to install and are significantly lighter, and would  
658 therefore be helpful when there are weight constraints. However, based on the very limited  
659 testing we did, PTFE fittings and tubing *may be* sufficient to store water for up to a single week,  
660 but on longer timescales (e.g. 27 days) we observed greater exchange and leaking than with the  
661 stainless steel fittings. We encourage any future user using this modification to rigorously test  
662 these fittings on a timescale appropriate for their application.

663



## 664 **6.1.2 Water vapor tests**

665 Our initial goal with the water vapor tests was to test whether the measured water vapor  
666 isotope values at the end of the two-week holding period were normally distributed about 0  
667 within the uncertainty limits of the water vapor probes (Oerter et al., 2016). This was a  
668 reasonable goal given the similarities in probe set-up and the plumbing design between the  
669 SWISS and the IsoWagon system (Oerter et al., 2016). But, the most salient result of the water  
670 vapor tests is that there is a consistent positive offset between the input isotope values and the  
671 isotope values measured at the end of the two-week experiments (Figs 4B, 5B). The positive  
672 offset in both  $\delta^{18}\text{O}$  and  $\delta^2\text{H}$  values is consistent across 11 different tests, using six different  
673 SWISS and three different input water isotope values. If there was alteration of original values  
674 due to leaky flasks, we might expect the  $\delta^{18}\text{O}$  and  $\delta^2\text{H}$  values to converge on the  $\delta^{18}\text{O}$  and  $\delta^2\text{H}$   
675 value of the atmosphere. For example, we might expect water vapor from the light water test to  
676 have the most significant change in isotope value, towards that of the ambient atmosphere.  
677 Instead, the consistency across >135 flasks, different starting water vapor isotope values, sample  
678 introduction methods, and multiple analytical sessions suggests that this difference is a function  
679 of the storage and measurement process. In particular, the normality of the distribution suggests  
680 whatever the origin of the offset is, there is a systematic bias that we can reliably correct for.

### 681 682 *6.1.2.1 Offset correction*

683 To correct our data for this offset, we chose to use the median value as an offset  
684 correction rather than the mean of the normal distribution, because the median is not biased by  
685 major outlier isotope values that reflect abnormal values that go beyond analytical noise, such as  
686 a slow but major leak that changes the values far beyond the basic offset seen in the dataset. The  
687 calculated average offset is 1.0‰ and 2.6‰ for  $\delta^{18}\text{O}$  and  $\delta^2\text{H}$ , respectively. After applying these  
688 values as an offset correction to the data, most flasks also fall within the uncertainty of the water  
689 vapor permeable probes ( $\delta^{18}\text{O} = \pm 0.5\text{‰}$  and  $\delta^2\text{H} = \pm 2.4\text{‰}$ , Oerter et al., 2016), and the values  
690 are distributed about 0 (Figs. 4C, 5C). However, the uncertainty of the SWISS system is higher  
691 than that of the probes alone. Based on the results of the water vapor tests, we estimate the  
692 uncertainty of the SWISS at  $\pm 0.9\text{‰}$  and  $\pm 3.7\text{‰}$  for  $\delta^{18}\text{O}$  and  $\delta^2\text{H}$ , respectively using the  
693 interquartile range (IQR) of the water vapor test results after removing outliers from the dataset.  
694 We prefer the IQR over the calculated standard deviation of the normal distribution, because  
695 IQR is not biased by outlier values. This level of uncertainty is large relative to other methods,  
696 but is sufficient for many critical zone applications, given the magnitude of seasonal variability  
697 in the top ~50 cm of a soil profile that can be observed in natural systems (e.g. Oerter et al.,  
698 2017; Quade et al., 2019). We also expect that uncertainties will decrease with future lab-based  
699 or near research facility testing and by comparing the SWISS against other soil water extraction  
700 methods.

701 The relationship between  $\delta^2\text{H}$  values and  $\delta^{18}\text{O}$  values in a dual-isotope plot provides  
702 insight into the mechanism driving the offset. Without an offset correction applied, the slope of  
703 the relationship between  $\delta^2\text{H}$  and  $\delta^{18}\text{O}$  is 3.14 ( $R^2 = 0.62$ ) (Supplemental Fig. 4). This slope is  
704 only slightly higher than evaporation under pure diffusion (Gonfiantini et al., 2018). This  
705 suggests that the offset is likely driven by diffusion and will likely vary according to climate of  
706 the lab. For example, in a dry climate like Colorado, the water vapor concentration in the flask is  
707 significantly higher than the atmosphere, creating a larger diffusive gradient potential than for a  
708 lab in a more humid climate. We therefore strongly encourage future users to test their SWISS  
709 under climate conditions similar for their applications. Further, we encourage users who might

710 use the SWISS as part of a tracer study that uses labeled heavy water to test the SWISS with  
711 labeled waters prior to their field experiments to verify reliability.

712

### 713 *6.1.2.2 Comparing sample introduction methods*

714 Supplemental figure 6 shows a kernel density estimate plot of the results from two water  
715 vapor test sessions, with the offset correction applied. During the March 2022 session, flasks  
716 were measured using the dead-end pull sample introduction method and during the August 2022  
717 session, flasks were measured using the dry air carrier gas sample introduction method. There is  
718 no significant difference in the measured difference between the two sample introduction  
719 methods. That said, we prefer the dry air carrier gas method, because it is far simpler to control  
720 the water vapor mixing ratio, and optimize the concentration to be around 25,000 ppm, which is  
721 the concentration at which the Picarro L2130-*i* is most reliable. The dry air carrier gas method  
722 also makes it easier to control for and monitor for condensation in the stainless-steel tubing and  
723 vapor impermeable tubing, which can bias a measurement.

724

### 725 *6.1.3 Field suitability tests*

726 The long dry air tests in the field are a useful complement to the shorter in-lab tests  
727 because they test the reliability of the system at field-deployment timescales. It is clear from the  
728 34 and 43 day tests that the flasks are reasonably resistant to leaks on the timescale of a normal  
729 four – six week deployment (Fig. 6A). These tests also give us confidence that flasks filled later  
730 in the sampling sequence do not take on an atmospheric signal prior to sampling. There are a few  
731 possibilities to explain the poorer performance of the Toblerone SWISS unit during the 52-day  
732 test. (Fig. 6A). The first is that there is a real threshold past which the SWISS are no longer able  
733 to retain samples. However, this explanation would suggest that there should be a gradual  
734 decrease in performance across the three tests, which we do not observe. The alternative  
735 explanation is that the poor performance is a result of inter-unit variability. The 52-day test was  
736 the first long-term test and was performed in August 2021. In August 2021, we were continuing  
737 to build new SWISS units and continuing to learn from each successive round of QA/QC, so it  
738 seems plausible that there were unidentified problems with the SWISS unit Toblerone that were  
739 solved before the water vapor tests in August 2022.

740 In figure 6B, the data show that the flasks preserved the  $\delta^{18}\text{O}$  value of both flash-  
741 evaporated and atmospheric water vapor over a seven-day period. One flask was removed from  
742 the dataset (flask eight), because there was visible condensation in the clear impermeable tubing  
743 during the measurement phase, with an increase of  $> 5\%$  for  $\delta^{18}\text{O}$  during the measurement  
744 period. The condensation appeared as small ( $<1$  mm) bubbles of water all along the impermeable  
745 tubing, but the bubbles were concentrated near the connection between the SWISS and the  
746 impermeable tubing. Notably, the two flasks whose  $\delta^{18}\text{O}$  values do not overlap within  
747 uncertainty are more negative than expected, rather than drifting towards atmospheric values or  
748 values expected from diffusive fractionation. In contrast to the  $\delta^{18}\text{O}$  values, only three flasks  
749 filled with flash evaporated water vapor overlap within uncertainty of the known  $\delta^2\text{H}$  values,  
750 while four of the five flasks overlap within uncertainty of the estimated atmosphere isotope  
751 value. The flasks tend to drift towards the value of the atmosphere, but retain the overall data  
752 pattern from the oxygen isotope values.

753 The relatively high failure rate of this ‘mock’ field test was somewhat surprising given  
754 the results of the water vapor tests done in the laboratory. Going into the test, we suspected that  
755 flasks six and eight were slightly leaky based on previous water vapor tests; these were flasks

756 that previously performed poorly, but did not ‘fail’ during the water vapor test. Once we  
757 collected the data, we compared the data for flasks six and eight to other flasks in the sequence.  
758 During the measurement of flask eight, we observed condensation in the sample introduction  
759 lines, and because the isotope values were so different relative to other flasks, we felt confident  
760 in our exclusion of flask eight. Flask six had  $\delta^{18}\text{O}$  and  $\delta^2\text{H}$  values similar to others from the same  
761 sampling source, and seemed to fall within the pattern as expected. Therefore, we chose to keep  
762 this data point in the dataset.

763 We hypothesize that one major problem with the mock field test dataset was the creation  
764 of condensation in the sampling lines, as others have experienced in their setups (e.g. Quade et  
765 al., 2019; Kühnhammer et al., 2019). Of particular interest are the flasks that had a lower than  
766 expected  $\delta^{18}\text{O}$  value (flasks four and nine). It is possible that those samples were also affected by  
767 condensation, but in contrast to flask eight, which was excluded because of condensation during  
768 measurement, we think that these samples may have been altered because of condensation at the  
769 sampling stage. During condensation, we expect that  $^{18}\text{O}$  will preferentially enter the liquid  
770 phase, and that the water vapor that enters the flask will have a lower than expected  $\delta^{18}\text{O}$  value.  
771 The unique advantage of the SWISS is that it can operate independently, but with that comes the  
772 trade-off that we cannot currently observe condensation in the lines during sample collection. To  
773 prevent condensation from forming, other users have warmed the impermeable tubing between  
774 the probes and the Picarro instrument. The ‘mock’ field test data suggest that in many situations  
775 it may be worthwhile to warm the transfer tubing, but this should be done in a way that does not  
776 alter the thermal structure of the soil, and in remote settings, can operate safely independently.

#### 777 ***6.1.4 Lessons learned and recommendations from the QA/QC and field suitability tests:***

778 Our QA/QC process was a relatively efficient way to test the soundness of the SWISS  
779 units. Through the QA/QC process we were able to identify problems with units, and  
780 appropriately address them before deploying units to the field. We strongly recommend that any  
781 user deploying SWISS to the field to undertake the same, or similar, QA/QC process.

782 The dry air test is a time-efficient and low-cost method for identifying flasks that are  
783 leaky and will not preserve the sampled water vapor isotope values. It is useful during the  
784 building stage to identify fittings that need to be tightened or flasks that need to be replaced, and  
785 therefore we recommend these tests as a required pre-deployment step for future SWISS units.  
786 We found that it was most time and energy efficient to move onto the next level of QA/QC once  
787 13 out of 15 flasks of a SWISS unit had passed the dry-air test, because frequently the remaining  
788 two flasks still had relatively low water vapor mole fractions (i.e. 500 – 700 ppm), and we could  
789 sufficiently tighten the fittings prior to the start of the water vapor tests for them to be successful.  
790 The dry air test is a low time and expense burden that can also be used to monitor SWISS units  
791 for normal wear-and-tear (e.g. a flask that cracked during transport) during deployment periods.  
792 Therefore, to ensure that SWISS units continue to operate as expected, we also recommend that  
793 dry air tests be done between field deployments on every SWISS unit. Lastly, we note that the  
794 dry air test could be modified based on available equipment (for example, if an instrument is  
795 available to measure trace atmospheric gases, that could be used instead).

796 Based on the results of the long, field dry air test, we recommend that the water vapor  
797 storage time doesn’t exceed 40 days for reliable results, or that the user undertake multiple dry  
798 air tests with either lower concentration benchmarks or longer duration if deployments may  
799 exceed 40 days.  
800

801 Overall, the quality control and quality assurance as well as the field suitability tests  
802 demonstrate that the SWISS units can retain the isotope values of water vapor collected using  
803 water vapor permeable probes. Like many other systems that measure dual isotopes (i.e.  $\delta^{18}\text{O}$   
804 and  $\delta^2\text{H}$ ), each system must be evaluated separately. In general, we interpret oxygen isotope data  
805 with a higher degree of confidence than the hydrogen isotope data. As the automation test  
806 revealed however, even when the absolute  $\delta^2\text{H}$  value is not correct, the general pattern can reveal  
807 information about soil water dynamics.

808 Finally, we opted to use a large flask volume because we hypothesize that it allows us to  
809 measure a sample for long enough on a CRDS that we get reliable data, without interacting with  
810 vapor bound to the flask walls. The drawback of this, however, is that we must sample soil water  
811 vapor for a relatively long period of time (45 minutes). In supplemental figure 7, we show that  
812 the sampling regime, and particularly the length of time we pump dry air through the tubing,  
813 does not significantly alter the soil moisture content of the soil. Additionally, we demonstrate  
814 that the sampling regime we use does not introduce significant memory effects.

815

## 816 **6.2 Field Deployments**

817 In Figure 7 we show the results of three field deployments completed during summer  
818 2022 (Table 3). At the Oglala National Grassland site, we used the SWISS unit named Lindt to  
819 collect samples. During the August 2022 water vapor test on Lindt, all  $\delta^{18}\text{O}$  values fall within  
820 uncertainty of the system, and nine of the fifteen  $\delta^2\text{H}$  values fall within uncertainty of the system.  
821 Therefore, we interpret the  $\delta^{18}\text{O}$  values with greater confidence and the  $\delta^2\text{H}$  values with lower  
822 confidence (Figs. 4C and 5C). We note that the  $\delta^{18}\text{O}$  and  $\delta^2\text{H}$  values broadly follow the same  
823 trends, and fall on the global meteoric water line (Figs. 7 and 8A). In general, soil water from 25  
824 cm had higher  $\delta^{18}\text{O}$  and  $\delta^2\text{H}$  values than soil water from both 50 and 75 cm (Fig. 8A). Given that  
825 4 of the 5 samples from 25 cm overlap with the GMWL and have a d-excess that overlaps with  
826  $10 \pm 2.6\text{‰}$ , the soil water from that depth may reflect summer precipitation with higher  $\delta^{18}\text{O}$  and  
827  $\delta^2\text{H}$  values. Soil water from 75 cm had intermediate  $\delta^{18}\text{O}$  and  $\delta^2\text{H}$  values for most of the study  
828 period, and soil water from 50 cm depth had the lowest  $\delta^{18}\text{O}$  and  $\delta^2\text{H}$  values for most of the  
829 study period, which may reflect a more mean-annual or winter precipitation biased value. Based  
830 on data available from the National Weather Service (Chadron, NE), there were likely significant  
831 precipitation events on 2022-06-25 and 2022-07-08 at the field site. There is a significant shift to  
832 lower  $\delta^{18}\text{O}$  values at a sampling depth of 25 cm between 2022-06-25 and 2022-06-29, as well as  
833 a marked increase in the d-excess value (Fig. 8A). We interpret this shift as infiltration of  
834 precipitation with lower  $\delta^{18}\text{O}$  values, which is supported by a return of d-excess values to  $\sim 10\text{‰}$   
835 (Fig. 8A). The National Weather Service reported 21.33 mm (0.84 inches) of rain at Chadron  
836 Municipal Airport, approximately 50 km from the study site on 2022-07-08, which likely was  
837 associated with at least some precipitation at our field site. Following the significant rain event  
838 on 2022-07-08, we observe a marked increase in the stable isotope value of water vapor from a  
839 sampling depth of 50 cm, towards values that are much closer to those at 25 cm depth. These  
840 data suggests that soil water isotopes at 50 cm in this silt-loam Aridisol may be fairly sensitive to  
841 large individual precipitation events, while at 75 cm soil water isotopes remain comparatively  
842 uniform. Future work should address how drought conditions, storm size, pore size distribution,  
843 and soil clay mineralogy influence the variability of soil water isotopes with depth.

844 At Briggsdale, CO we used the SWISS named Raclette to collect soil water vapor  
845 samples. Data from 25 cm depth at Briggsdale, CO were discarded because the water vapor mole  
846 fraction was much lower than would be expected given the soil temperature (i.e.  $< 15,000$  ppm).

847 The gravimetric water concentration (GWC) at that soil depth at the time of sampling was  
848 approximately 4% through the sampling period. Future work should include a multiple-method  
849 (e.g. cryogenic extraction, centrifugation, etc.) comparison of soil water isotopes at low water  
850 contents to better understand what these samples might represent, and if they are actually  
851 representative of soil conditions.

852 Based on the results of the August 2022 water vapor test done on Raclette where all  
853 flasks fell within uncertainty of the SWISS system for both  $\delta^{18}\text{O}$  and  $\delta^2\text{H}$ , except for flask 11  
854 (Figs. 4C and 5C), we interpret all data with greater confidence. Flask 11 corresponds to the 25  
855 cm depth sample from 2022-07-27, and was already culled from the dataset because of low water  
856 vapor mole fraction associated with the very dry soil. The soil water  $\delta^{18}\text{O}$  and  $\delta^2\text{H}$  values from a  
857 sampling depth of 50 cm and 75 cm overlap within uncertainty, but the soil water  $\delta^{18}\text{O}$  and  $\delta^2\text{H}$   
858 values from 50 cm are higher than the isotope values from 75 cm. All of the data from each  
859 sampling depth group (i.e. 50 cm and 75 cm) overlap within uncertainty, conforming to the  
860 expectation that soil water from these sampling depths should be fairly invariant (e.g. Oerter et  
861 al., 2019). There were precipitation events at the study site on 2022-07-24, 2022-07-28 and  
862 2022-07-31. It is possible that the slight negative shift in both  $\delta^{18}\text{O}$  and  $\delta^2\text{H}$  on 2022-08-01  
863 reflects infiltration of precipitation to those depths, but this is not certain given that all of the  
864 measurements from within a sampling depth overlap within uncertainty.

865 At Seibert, CO we used the SWISS named Toblerone to collect soil water vapor samples.  
866 The soil water isotope data from 75 cm depth at this site offer a few useful lessons for future  
867 users. The two key observations of the data from 75 cm depth are that the  $\delta^{18}\text{O}$  and  $\delta^2\text{H}$  values  
868 are much higher than the ones from other two sampling depths, and that the  $\delta^2\text{H}$  and  $\delta^{18}\text{O}$  values  
869 do not move in parallel with each other. While measuring these samples we observed  
870 condensation in the impermeable tubing at the point where the SWISS connects to the  
871 impermeable tubing. Additionally, when we heated the stainless-steel tubing that connects the  
872 tubing flask and Valco valve we observed a rapid increase in water vapor mole fraction (1000's  
873 of ppm over <30 seconds) that was accompanied by a rise in stable isotope value. During these  
874 measurements, we were rarely able to get a stable isotope value measurement window, and  
875 instead the stable isotope value of the vapor increased continually through the measurement. It is  
876 for these reasons that we feel confident in discarding the stable isotope data from 2022-06-19 –  
877 2022-06-29. The final measurement from 75 cm depth on 2022-07-04 approaches a reasonable  
878 isotope value when compared to isotope values from the other two depths, and that sample had  
879 fewer condensation problems during measurement. However, because we have no sequential  
880 context for what a reasonable value for this depth is, we discarded that value as well. For that  
881 final 75 cm sample, we were more successful because we warmed the entire length the vapor  
882 impermeable tubing, as well as the stainless-steel tubing, flask, and Valco valve evenly so that  
883 there were no temperature gradients across the vapor path. If the condensation had only been in  
884 the impermeable tubing it would have been much easier to successfully analyze these samples by  
885 just closing off the flask and running dry air through the tubing to remove condensation, but  
886 because condensation was also occurring in the stainless-steel tubing between the flask and  
887 Valco valve, this was not possible. It remains unclear why condensation was such a significant  
888 problem for samples from that depth as opposed to samples from different depths in the same  
889 SWISS. Future work should include further testing of the SWISS across different water contents  
890 and temperatures to better understand why the phenomenon may have occurred.

891 Based on the results of the August 2022 water vapor test done on Toblerone, we interpret  
892 all data from 50 cm and 25 cm depth with high confidence, except for Flask 3, which is the 50

893 cm sample from 2022-06-19 (Figs. 4C and 5C). Unlike data from the other two field sites, soil  
894 water from 25 cm and 50 cm overlap within uncertainty. There were two precipitation events at  
895 the field site during the sampling period on 2022-06-25 and 2022-07-01, but both events were  
896 quite small (<0.5 mm, CoAgMet). There is no significant influence of the precipitation events on  
897 the  $\delta^{18}\text{O}$  and  $\delta^2\text{H}$  values. The >1.0‰ increase in  $\delta^{18}\text{O}$  values on 2022-06-29 is surprising given  
898 that there is not a comparable magnitude increase in  $\delta^2\text{H}$  value, and that the values measured  
899 from 2022-07-04 more closely match the  $\delta^{18}\text{O}$  and  $\delta^2\text{H}$  values from the two earlier sampling  
900 days. There are two potential explanations for this data. First, that this shift is a real signal from  
901 an evaporation driven increase in the  $\delta^{18}\text{O}$  value, and the shift back to a lower  $\delta^{18}\text{O}$  value on  
902 2022-07-04 is due to the infiltration of precipitation, which could also explain the low d-excess  
903 value associated with this measurement (Supplemental Fig. 8). The second possible explanation  
904 is that the 25 cm sample from 2022-06-29 is influenced by condensation at the time of sampling.  
905 Dew point at the field site on 2022-06-29 significantly decreased as compared to the other  
906 sampling days to a monthly minimum of 20.6°C (CoAgMet). It is possible that environmental  
907 conditions encouraged the formation of condensation in the impermeable tubing at the time of  
908 sampling; if there was residual condensation in the impermeable tubing then its possible we  
909 were partially sampling a heavier condensed water. There were no obvious signs of condensation  
910 during the time of measurement in the lab. These results highlight the utility of having broad  
911 contextual environmental data to aid in the interpretation of soil water isotope data.

912 All together, these three soil water isotope datasets demonstrate two main findings. First,  
913 data from these samples show that the differences between field sites are easily resolvable using  
914 the SWISS. For example, at 50 cm depth the oxygen isotopes range between -14.4 to -16.3‰, -  
915 9.9 to -10.3‰, and -7.4 to -9.3‰ for the Oglala, Briggsdale and Seibert sites, respectively. These  
916 differences likely reflect differences in the stable isotope composition of precipitation and  
917 infiltration and evaporation dynamics. Second, the sample data retrieved from a SWISS are  
918 sufficiently precise to be able to meaningfully resolve vertical profile soil water isotope data. For  
919 example, at the Oglala National Grassland field site, soil water from 25 cm clearly has higher  
920  $\delta^{18}\text{O}$  and  $\delta^2\text{H}$  values as compared to soil water from a depth of 50 and 75 cm.

921

### 922 **6. 3 Future improvements and future work**

923 One significant SWISS unit hardware improvement that could be made would be to  
924 install a heating implement to the flasks. One source of uncertainty on the current system is the  
925 potential effect of uneven heating of the flasks prior to measurement which may create  
926 temperature gradients that are large enough to allow for condensation when warm vapor meets a  
927 spot slightly colder than dew point. This could be improved in subsequent iterations of the  
928 SWISS with the addition of heat tape or blankets that can deliver controlled heat and create  
929 consistent temperatures. This improvement would also help limit the amount of manual  
930 intervention needed during measurement, and could improve automation of flask measurement.  
931 Additionally, finding a way to safely and automatically heat the impermeable tubing that  
932 connects the water vapor probes and the SWISS in a way that doesn't change the inherent  
933 thermal structure of the soil, and is safe for unmonitored use, would help to prevent the  
934 formation of condensation in the field and reduce the uncertainties related to sampling as well as  
935 the number of samples that need to be discarded.

936 We have made a few improvements to the automation system that were not implemented  
937 for the data presented in this contribution, but will be part of future deployments. First, we will  
938 track conditions inside the SWISS with a temperature and relative humidity sensor inside the

939 case. Second, we plan to eliminate the power inverter by powering both the Valco valve and  
940 mass flow controller with VDC using a power step up controller. Lastly, we will add an IoT  
941 cellular router to be able to remotely monitor and control the SWISS units. This would be  
942 particularly helpful if there is a sampling day that is unexpectedly cold or when the dew point at  
943 the field site is unexpectedly low and we expect condensation to form more readily in the field,  
944 or if there is a precipitation event that we are interested in capturing, because with the IoT  
945 cellular router we could remotely alter the sampling plan.

946 While the improvements and additional testing we have done to the SWISS in this  
947 contribution represent a significant step forward, additional work should be done to make the  
948 system more useable by the ecohydrology community. We have rigorously tested the SWISS in  
949 the lab, and demonstrated a few ways in which the SWISS can fail in field settings. A full  
950 comparison of how soil water isotope data collected using a SWISS as compared to other in situ  
951 (both vapor probes and lysimeter) and destructive sampling methods would shed more light on  
952 the accuracy and precision of our system, and the applicability of our lab-based experiments to  
953 the field. These experiments should be carefully designed with considerations of soil grain size,  
954 soil water content, expected isotope values, and climate. Additionally, we plan to test SWISS  
955 unit resilience during air travel so that these units can be used at field sites that are not within  
956 driving distance of a research facility.

## 957 **Conclusions**

958 We presented the evolution of the soil water isotope storage system (SWISS) from a  
959 prototype to a fully built out and tested system. We also presented a quality control and quality  
960 assurance procedure that we strongly recommend future users undertake to ensure the reliable  
961 storage of soil water vapor over long time periods (up to 40 days). In addition, these quality  
962 control and quality assurance tests shed light on the accuracy and precision of the SWISS. After  
963 applying an offset correction, we determined the precision of the SWISS to be  $\pm 0.9\%$  and  
964  $\pm 3.7\%$  for  $\delta^{18}\text{O}$  and  $\delta^2\text{H}$ , respectively. In a field setting, flasks reliably resist atmospheric  
965 intrusion. Additionally, the proposed sampling schema does not introduce significant memory  
966 effects. Lastly, we demonstrated that the current precision of the SWISS still allows us to  
967 distinguish between field sites and between soil water dynamics within a single soil column.  
968 Taken as a whole, these data show that the SWISS can be used as a tool to answer many  
969 emerging ecohydrological questions, and will enhance researchers' ability to collect soil water  
970 isotope datasets from more remote and traditionally understudied field sites.

## 971 **Acknowledgements**

972 We thank the numerous field assistants who helped to make the field work presented in  
973 this paper possible, including Spencer Burns, Anne Fetrow, Sarah Brookins, Juliana Olsen-  
974 Valdez, and Haley Brumberger. We acknowledge that both field work and laboratory work for  
975 this study were done on the traditional territories and ancestral homelands of the Arapahoe, Ute  
976 and Cheyenne peoples. This work was supported by startup funding from CU Boulder and NSF  
977 funding from grant EAR-2023385 awarded to K. Snell. Additionally, this work was supported by  
978 the University of Colorado Boulder Beverly Sears Research Grant and the Clay Minerals Society  
979 Graduate Student Research Grant both awarded to R. Havranek. CUBES-SIL is a CU Boulder  
980 Core Facility associated with RRID: SCR\_019300.

981  
982 **Author contribution**  
983 Rachel E. Havranek: conceptualization, methodology, investigation, formal analysis, funding  
984 acquisition, writing – wrote original draft, review and editing. Kathryn E. Snell:  
985 conceptualization, methodology, writing – review & editing, funding acquisition. Sebastian H.  
986 Kopf: conceptualization, methodology, writing – review & editing. Brett Davidheiser-Kroll:  
987 conceptualization, methodology, writing – review & editing. Valerie Morris: methodology,  
988 writing – review & editing. Bruce Vaugh: methodology, writing – review & editing.  
989  
990 **Competing interests**  
991 The authors declare no competing interests.



992 **Works Cited**

- 993 Beyer, M., Kühnhammer, K., & Dubbert, M.: In situ measurements of soil and plant water  
994 isotopes: a review of approaches, practical considerations and a vision for the future.  
995 Hydrology and Earth System Sciences, 24, 4413–4440  
996 <https://doi.org/https://doi.org/10.5194/hess-24-4413-2020>, 2020.
- 997 Bowen, G. J., Cai, Z., Fiorella, R. P., & Putman, A. L.: Isotopes in the Water Cycle: Regional- to  
998 Global-Scale Patterns and Applications. Annual Review of Earth and Planetary Sciences,  
999 47(1), 453–479, <https://doi.org/10.1146/annurev-earth-053018-060220>, 2019
- 1000 Bowen, G. J., Putman, A., Brooks, J. R., Bowling, D. R., Oerter, E. J., & Good, S. P.: Inferring  
1001 the source of evaporated waters using stable H and O isotopes. Oecologia, 187(4), 1025–  
1002 1039, <https://doi.org/10.1007/s00442-018-4192-5>, 2018.
- 1003 Brooks, J. R., Barnard, H. R., Coulombe, R., & McDonnell, J. J.: Ecohydrologic separation of  
1004 water between trees and streams in a Mediterranean climate. Nature Geoscience, 3(2), 100–  
1005 104, <https://doi.org/10.1038/ngeo722>, 2010.
- 1006 CoAgMet, Colorado Climate Center, Colorado State University, Fort Collins, CO, USA.  
1007 <https://coagmet.colostate.edu/>, last access: 25 April 2023.
- 1008 Dawson, T. E., & Ehleringer, J. R.: Streamside trees that do not use stream-water: evidence from  
1009 hydrogen isotopes ratios. Nature, 350(March), 335–337, <https://doi.org/10.1038/350335a0>,  
1010 1991.
- 1011 Gaj, M., Beyer, M., Koeniger, P., Wanke, H., Hamutoko, J., & Himmelsbach, T.: In-situ  
1012 unsaturated zone stable water isotope ( $^2\text{H}$  and  $^{18}\text{O}$ ) measurements in semi-arid environments  
1013 using tunable off-axis integrated cavity output spectroscopy. Hydrology and Earth System  
1014 Sciences Discussions, 12(6), 6115–6149, <https://doi.org/10.5194/hessd-12-6115-2015>, 2015
- 1015 Gaj, M., Beyer, M., Koeniger, P., Wanke, H., Hamutoko, J., & Himmelsbach, T.: In situ  
1016 unsaturated zone water stable isotope ( $^2\text{H}$  and  $^{18}\text{O}$ ) measurements in semi-arid  
1017 environments: A soil water balance. Hydrology and Earth System Sciences, 20(2), 715–731.  
1018 <https://doi.org/10.5194/hess-20-715-2016>, 2016.
- 1019 Gessler, A., Bächli, L., Rouholahnejad Freund, E., Treydte, K., Schaub, M., Haeni, M., Weiler,  
1020 M., Seeger, S., Marshall, J., Hug, C., Zweifel, R., Hagedorn, F., Rigling, A., Saurer, M., &  
1021 Meusburger, K.: Drought reduces water uptake in beech from the drying topsoil, but no  
1022 compensatory uptake occurs from deeper soil layers. New Phytologist, 233(1), 194–206,  
1023 <https://doi.org/10.1111/nph.17767>, 2022.
- 1024 Gómez-Navarro, C., Pataki, D. E., Bowen, G. J., & Oerter, E. J.: Spatiotemporal variability in  
1025 water sources of urban soils and trees in the semiarid, irrigated Salt Lake Valley.  
1026 Ecohydrology, 12(8), <https://doi.org/10.1002/eco.2154>, 2019.
- 1027 Gonfiantini, R., Wassenaar, L. I., Araguas-Araguas, L., & Aggarwal, P. K.: A unified Craig-  
1028 Gordon isotope model of stable hydrogen and oxygen isotope fractionation during fresh or  
1029 saltwater evaporation, Geochimica et Cosmochimica Acta, 235, 224–236.  
1030 <https://doi.org/10.1016/j.gca.2018.05.020>, 2018.
- 1031 Good, S. P., Noone, D., & Bowen, G. J.: Hydrologic connectivity constrains partitioning of  
1032 global terrestrial water fluxes. Science, 349(6244), 175–177,  
1033 <https://doi.org/10.1126/science.aaa5931>, 2015.

- 1034 Green, M. B., Laursen, B. K., Campbell, J. L., Mcguire, K. J., & Kelsey, E. P.: Stable water  
 1035 isotopes suggest sub-canopy water recycling in a northern forested catchment. *Hydrological*  
 1036 *Processes*, 29(25), 5193–5202, <https://doi.org/10.1002/hyp.10706>, 2015
- 1037 Groh, J., Stumpp, C., Lücke, A., Pütz, T., Vanderborght, J. and Vereecken, H.: Inverse  
 1038 estimation of soil hydraulic and transport parameters of layered soils from water stable  
 1039 isotope and lysimeter data. *Vadose Zone Journal*, 17(1), 1-19,  
 1040 <https://doi.org/10.2136/vzj2017.09.0168>, 2018.
- 1041 Gupta, P., Noone, D., Galewsky, J., Sweeney, C., and Vaughn, B.H.: Demonstration of high-  
 1042 precision continuous measurements of water vapor isotopologues in laboratory and remote  
 1043 field deployments using wavelength-scanned cavity ring-down spectroscopy (WS-CRDS)  
 1044 technology. *Rapid Com. in Mass Spectrometry*, 23, 2534-2542,  
 1045 <https://doi.org/10.1002/rcm.4100>, 2009
- 1046 Harms Sarah M, & Ludwig, T. K.: Retention and removal of nitrogen and phosphorus in saturated  
 1047 soils of arctic hillslopes. *Biogeochemistry*, 127, 291–304 [https://doi.org/10.1007/s10533-](https://doi.org/10.1007/s10533-016-0181-0)  
 1048 [016-0181-0](https://doi.org/10.1007/s10533-016-0181-0), 2016.
- 1049 Havranek, R. E., Snell, K. E., Davidheiser-Kroll, B., Bowen, G. J., & Vaughn, B.: The Soil  
 1050 Water Isotope Storage System (SWISS): An integrated soil water vapor sampling and  
 1051 multiport storage system for stable isotope geochemistry. *Rapid Communications in Mass*  
 1052 *Spectrometry*, 34(12), 1–11. <https://doi.org/10.1002/rcm.8783>, 2020
- 1053 Hinckley, E.-L. S., Barnes, R. T., Anderson, S. P., Williams, M. W., & Bernasconi, S. M.:  
 1054 Nitrogen retention and transport differ by hillslope aspect at the rain-snow transition of the  
 1055 Colorado Front Range. *Journal of Geophysical Research: Biogeosciences*, 119, 12811896.  
 1056 <https://doi.org/10.1002/2013JG002588>, 2014.
- 1057 Kübert, A., Paulus, S., Dahlmann, A., Werner, C., Rothfuss, Y., Orłowski, N., & Dubbert, M. :  
 1058 Water Stable Isotopes in Ecohydrological Field Research : Comparison Between In Situ and  
 1059 Destructive Monitoring Methods to Determine Soil Water Isotopic Signatures. *Frontiers in*  
 1060 *Plant Science*, 11(April), 1–13, <https://doi.org/10.3389/fpls.2020.00387>, 2020.
- 1061 Kühnhammer, K., Dahlmann, A., Iraheta, A., Gerchow, M., Birkel, C., Marshall, J. D., & Beyer,  
 1062 M.: Continuous in situ measurements of water stable isotopes in soils, tree trunk and root  
 1063 xylem: Field approval. *Rapid Comm. in Mass Spec.*, 36(5).  
 1064 <https://doi.org/10.1002/rcm.9232>, 2022.
- 1065 Magh, R.K., Gralher, B., Herbstritt, B., Kübert, A., Lim, H., Lundmark, T. and Marshall, J.:  
 1066 Technical note: Conservative storage of water vapour–practical in situ sampling of stable  
 1067 isotopes in tree stems, *Hydrol. Earth Syst. Sci.*, 26, 3573–3587, [https://doi.org/10.5194/hess-](https://doi.org/10.5194/hess-26-3573-2022)  
 1068 [26-3573-2022](https://doi.org/10.5194/hess-26-3573-2022), 2022.
- 1069 Mahindawansa, A., Orłowski, N., Kraft, P., Rothfuss, Y., Racela, H., & Breuer, L.:  
 1070 Quantification of plant water uptake by water stable isotopes in rice paddy systems. *Plant*  
 1071 *and Soil*, 429(1–2), 281–302. <https://doi.org/10.1007/s11104-018-3693-7>, 2018
- 1072 Oerter, E. J., Perelet, A., Pardyjak, E., & Bowen, G. J.: Membrane inlet laser spectroscopy to  
 1073 measure H and O stable isotope compositions of soil and sediment pore water with high  
 1074 sample throughput. *Rapid Communications in Mass Spectrometry*, 31(1), 75–84,  
 1075 <https://doi.org/10.1002/rcm.7768>, 2016.

- 1076 Oerter, E. J., & Bowen, G. J.: In situ monitoring of H and O stable isotopes in soil water reveals  
1077 ecohydrologic dynamics in managed soil systems. *Ecohydrology*, 10(4), 1–13,  
1078 <https://doi.org/10.1002/eco.1841>, 2017
- 1079 Oerter, E. J., & Bowen, G. J.: Spatio-temporal heterogeneity in soil water stable isotopic  
1080 composition and its ecohydrologic implications in semiarid ecosystems. *Hydrological*  
1081 *Processes*, March, 1–15. <https://doi.org/10.1002/hyp.13434>, 2019
- 1082 Peterson, B. J., & Fry, B.: Stable Isotopes in Ecosystem Studies. *Annual Reviews of Ecology and*  
1083 *Systematics*, 18, 293–320, <http://www.jstor.org/stable/2097134>, 1987.
- 1084 Quade, M., Klosterhalfen, A., Graf, A., Brüggemann, N., Hermes, N., Vereecken, H., &  
1085 Rothfuss, Y.: In-situ monitoring of soil water isotopic composition for partitioning of  
1086 evapotranspiration during one growing season of sugar beet (*Beta vulgaris*). *Agri. and*  
1087 *Forest Met.*, 266–267, 53–64. <https://doi.org/10.1016/j.agrformet.2018.12.002>, 2019.
- 1088 Quade, M., Brüggemann, N., Graf, A., Vanderborght, J., Vereecken, H., & Rothfuss, Y.:  
1089 Investigation of Kinetic Isotopic Fractionation of Water during Bare Soil Evaporation.  
1090 *Water Resources Research*, 54(9), 6909–6928, <https://doi.org/10.1029/2018WR023159>,  
1091 2018.
- 1092 Rothfuss, Y., Vereecken, H., & Brüggemann, N.: Monitoring water stable isotopic composition  
1093 in soils using gas-permeable tubing and infrared laser absorption spectroscopy. *Water*  
1094 *Resources Research*, 49, 3747–3755, <https://doi.org/10.1002/wrcr.20311>, 2013.
- 1095 Rothfuss, Y., Merz, S., Vanderborght, J., Hermes, N., Weuthen, A., Pohlmeier, A., Vereecken,  
1096 H., & Brüggemann, N.: Long-term and high-frequency non-destructive monitoring of water  
1097 stable isotope profiles in an evaporating soil column. *Hydrol. Earth Syst. Sci.*, 19(10),  
1098 4067–4080, <https://doi.org/10.5194/hess-19-4067-2015>, 2015.
- 1099 Rothfuss, Y., Quade, M., Brüggemann, N., Graf, A., Vereecken, H., & Dubbert, M.: Reviews  
1100 and syntheses: Gaining insights into evapotranspiration partitioning with novel isotopic  
1101 monitoring methods., *Biogeosciences*, 18 (12), 3701–3732, [https://doi.org/10.5194/bg-18-](https://doi.org/10.5194/bg-18-3701-2021)  
1102 [3701-2021](https://doi.org/10.5194/bg-18-3701-2021), 2021.
- 1103 Rozmiarek, K. S., Vaughn, B. H., Jones, T. R., Morris, V., Skorski, W. B., Hughes, A. G.,  
1104 Elston, J., Wahl, S., Faber, A. K., & Steen-Larsen, H. C.: An unmanned aerial vehicle  
1105 sampling platform for atmospheric water vapor isotopes in polar environments.  
1106 *Atmospheric Measurement Techniques*, 14(11), 7045–7067, [https://doi.org/10.5194/amt-14-](https://doi.org/10.5194/amt-14-7045-2021)  
1107 [7045-2021](https://doi.org/10.5194/amt-14-7045-2021), 2021.
- 1108 Seeger, S., & Weiler, M.: Temporal dynamics of tree xylem water isotopes: In situ monitoring  
1109 and modeling. *Biogeosciences*, 18(15), 4603–4627, [https://doi.org/10.5194/bg-18-4603-](https://doi.org/10.5194/bg-18-4603-2021)  
1110 [2021](https://doi.org/10.5194/bg-18-4603-2021), 2021.
- 1111 Soderberg, K., Good, S. P., Wang, L., & Caylor, K.: Stable Isotopes of Water Vapor in the  
1112 Vadose Zone: A Review of Measurement and Modeling Techniques. *Vadose Zone Journal*,  
1113 11(3), <https://doi.org/10.2136/vzj2011.0165>, 2012.
- 1114 Soil Survey Staff, Natural Resources Conservation Service, United States Department of  
1115 Agriculture. Soil Series Classification Database. <https://websoilsurvey.nrcs.usda.gov/>.  
1116 Accessed 09 October 2022.

- 1117 Sprenger, M., Leistert, H., Gimbei, G., & Weiler, M., Illuminating hydrological processes at the  
1118 soil-vegetation-atmosphere interface with water stable isotopes. *Reviews in Geophysics*, 54,  
1119 674–704, <https://doi.org/10.1002/2015RG000515>, 2016.
- 1120 Sprenger, M., & Allen, S. T.: What Ecohydrologic Separation Is and Where We Can Go With It.  
1121 In *Water Resources Research* (Vol. 56, Issue 7). Blackwell Publishing Ltd.  
1122 <https://doi.org/10.1029/2020WR027238>, 2020.
- 1123 Stumpp, C., Stichler, W., Kandolf, M. and Šimůnek, J.: Effects of land cover and fertilization  
1124 method on water flow and solute transport in five lysimeters: A long-term study using stable  
1125 water isotopes. *Vadose Zone Journal*, 11(1), <https://doi.org/10.2136/vzj2011.0075>, 2012.
- 1126 Theis, D. E., Saurer, M., Blum, H., Frossard, E., & Siegwolf, R. T. W.: A portable automated  
1127 system for trace gas sampling in the field and stable isotope analysis in the laboratory. *Rapid*  
1128 *Communications in Mass Spectrometry*, 18(18), 2106–2112,  
1129 <https://doi.org/10.1002/rcm.1596>, 2004.
- 1130 Vereecken, H., Amelung, W., Bauke, S. L., Bogaen, H., Brüggemann, N., Montzka, C.,  
1131 Vanderborght, J., Bechtold, M., Blöschl, G., Carminati, A., Javaux, M., Konings, A. G.,  
1132 Kutsche, J., Neuweiler, I., Or, D., Steele-Dunne, S., Verhoef, A., Young, M., & Zhang, Y.:  
1133 Soil hydrology in the Earth system. *Nature Reviews Earth & Environment*, 3, 573-587,  
1134 <https://doi.org/10.1038/s43017-022-00324-6>, 2022.
- 1135 Volkmann, T. H. M., & Weiler, M.: Continual in situ monitoring of pore water stable isotopes in  
1136 the subsurface. *Hydrology and Earth System Sciences*, 18(5), 1819–1833,  
1137 <https://doi.org/10.5194/hess-18-1819-2014>, 2014.
- 1138 Volkmann, T. H. M., Haberer, K., Gessler, A., & Weiler, M., High-resolution isotope  
1139 measurements resolve rapid ecohydrological dynamics at the soil-plant interface. *New*  
1140 *Phytologist*, 210(3), 839–849. <https://doi.org/10.1111/nph.13868>, 2016.
- 1141 Wassenaar, L. I., Hendry, M. J., Chostner, V. L., & Lis, G. P.: High resolution pore water  $\delta^2\text{H}$   
1142 and  $\delta^{18}\text{O}$  measurements by  $\text{H}_2\text{O}_{(\text{liquid})}$ - $\text{H}_2\text{O}_{(\text{vapor})}$  equilibration laser  
1143 spectroscopy. *Environmental Science and Technology*, 42(24), 9262–9267.  
1144 <https://doi.org/10.1021/es802065s>, 2008.
- 1145 Zhao, P., Tang, X., Zhao, P., Wang, C. and Tang, J., 2013. Identifying the water source for  
1146 subsurface flow with deuterium and oxygen-18 isotopes of soil water collected from tension  
1147 lysimeters and cores. *Journal of Hydrology*, 503, 1-10,  
1148 <https://doi.org/10.1016/j.jhydrol.2013.08.033>, 2013.
- 1149 Zimmermann, U., Munnich, K. O., & Roether, W.: Tracers Determine Movement of Soil  
1150 Moisture and Evapotranspiration, *Science*, 152(3720), 346–347.  
1151 <https://doi.org/10.1126/science.152.3720.346>, 1966.
- 1152
- 1153